Integral quantification and phase space analysis of heat transfer in a particle-laden shearless turbulent flow

Hamid Reza Zandi Pour [1,2,*] Perry L. Johnson [3,†] and Michele Iovieno [2,‡]
[1] *Dipartimento di Fisica and INFN - Università degli Studi di Torino, Via Pietro Giuria, 1, 10125 Torino, Italy*
[2] *Politecnico di Torino, Dipartimento di Ingegneria Meccanica e Aerospaziale, Corso Duca degli Abruzzi 24, 10129 Torino, Italy*
[3] *University of California, Irvine, Samueli School of Engineering, Irvine, California 92697, USA*

(Received 25 July 2025; accepted 12 January 2026; published 23 February 2026)

We present a discussion of the enthalpy transport at the interface between two homothermal regions in a particle-laden turbulent flow, in order to quantify the role of inertial particles and of fluid-particle thermal interaction. We use a phase-space analysis of particles in a reduced phase space, and a formulation of a moment of total enthalpy integral (MTEI) applied to data from direct numerical simulations (DNS) at a Taylor microscale Reynolds number equal to 56 in a thermally coupled two-way regime. This allows us to identify the main features of particle statistics and to measure the effects of particle inertia and turbulent convection of the heat transfer, providing a quantitative and interpretable evaluation of the process which does not require any hypothesis of self-similarity. We show how particles dominate the transport mechanisms, bridging enthalpy across eddy structures, in particular when their Stokes number approaches unity, making them accumulate across temperature fronts.

DOI: 10.1103/l7cm-vszk

I. INTRODUCTION

Understanding the interplay between fluid turbulence and suspended inertial particles is essential for a wide range of environmental and industrial applications, including atmospheric processes, pollutant dispersion, spray cooling, combustion, and cloud microphysics. Compared to single-phase, nonisothermal turbulent flows, particle-laden turbulence involves additional multiscale and interphase processes that strongly affect heat, mass, and momentum transport. These include inertia and thermal inertia filtering, caustics and thermal caustics formation, and particle-fluid feedback mechanisms, which together make the physics of heat transfer in such flows considerably more complex.

Recent research has made progress in quantifying these processes through numerical simulations, experiments, and by developing novel theoretical models. For example, Saito *et al.* [1] derived an analytical prediction for the modulation of fluid temperature fluctuations by particles, using a

*Contact author: hamid.zandipour@polito.it, hamidreza.zandipour@unito.it
†Contact author: perry.johnson@uci.edu
‡Contact author: michele.iovieno@polito.it

Published by the American Physical Society under the terms of the Creative Commons Attribution 4.0 International license. Further distribution of this work must maintain attribution to the author(s) and the published article's title, journal citation, and DOI.

Langevin model for fluid temperature fluctuations along the Lagrangian trajectories of individual particles. Their model successfully predicted the direct numerical simulation (DNS) results by Carbone *et al*. [2]. Similarly, Carbone *et al*. have analyzed the modification of scalar statistics by particles in homogeneous, isotropic turbulence, identifying systematic effects of particle inertia and thermal response times on scalar intermittency [2,3]. Although these works have advanced our understanding of multiscale fluid-particle thermal interactions, they have primarily considered isotropic, statistically homogeneous, and steady fluid temperature and velocity fields. By contrast, many physically relevant flows involve strong inhomogeneities, anisotropy, and temporal evolution, features that can fundamentally alter the interaction mechanisms.

A variety of mechanisms shape the distribution and dynamics of inertial particles in turbulence. Preferential concentration, or clustering, depends on how particle inertia couples with turbulent eddies: heavy particles preferentially accumulate in high-strain/low-vorticity regions, while light particles do the opposite [4–6]. Turbulence-induced clustering, which arises from particle inertia, causes particles to accumulate near strong fluid temperature gradients, i.e., at temperature fronts, as reported by Bec *et al*. [7], leading to thermally biased sampling. Turbophoresis, recently revisited by Bec *et al*. [8], causes particles to be ejected from regions of strong activity and accumulate in less turbulent areas due to intrinsic instantaneous non-uniformities of the inertial range. Relatedly, the sweep-stick mechanism generalizes the centrifugal effect of vortices, linking particle clustering to their response times across inertial-range scales [9,10]. At very high Reynolds numbers, DNS studies confirmed strong correlations between particle positions and nearly zero-acceleration points in the flow, reinforcing this picture. Another phenomenon of central importance is the formation of caustics in particle velocity fields. For particles with a finite Stokes number St, and more frequently for $\mathrm{St} \gtrsim 1$, trajectories may cross in phase space, leading to multivalued particle velocities at the same position and generating large velocity differences between nearby particles [11,12]. Extending this concept, Zandi Pour *et al*. [13] recently developed a theory of thermal caustics, based on the dynamics of particle temperature gradients, providing a new theoretical framework that extends earlier treatments [1,2].

While these mechanisms are well understood in the context of isotropic turbulence, how they manifest in inhomogeneous, anisotropic, and unsteady thermal fields remains an open question. The majority of existing studies assume isotropic and homogeneous temperature and velocity fields, which simplifies both theory and numerical analysis. However, in realistic flows, scalar fields are rarely homogeneous or steady. For example, scalar mixing layers exhibit strong anisotropy, intermittency, and scale-dependent dynamics. As Warhaft noted [14], even in homogeneous and isotropic turbulence, the presence of a mean scalar gradient leads to deviations from local isotropy, such as finite skewness in transverse scalar derivatives [15]. Direct numerical simulations of scalar mixing layers further reveal the development of sharp intermittent fronts and $-5/3$ inertial-range spectra [16]. Thus, a systematic investigation of particle-scalar interactions in inhomogeneous, time-developing configurations is needed to bridge the gap between idealized homogeneous turbulence and more realistic thermally inhomogeneous flows.

We address this problem by studying a time-developing thermal mixing layer. Specifically, we consider two initially homothermal regions advected by a statistically steady, homogeneous, isotropic, incompressible velocity field, which generates a turbulent mixing layer in the intervening region. The fluid temperature is treated as a passive scalar, with temperature differences sufficiently small to avoid buoyancy effects. The mixing layer thickness grows in time and, after an initial transient, evolves diffusively, suggesting the possibility of self-similar growth [17–19]. Particles are modeled as identical spheres with a finite thermal capacity. Advected by the turbulent flow, they interact dynamically and thermally with both the mean temperature gradient and local intermittent fluctuations. This configuration, although idealized, captures the essential features of inhomogeneous, anisotropic, and unsteady scalar fields while retaining statistical stationarity of the velocity field.

The aim of this study is to investigate the role of inertial particles in the thermal transport across a turbulent mixing layer. We pursue this through two complementary approaches:

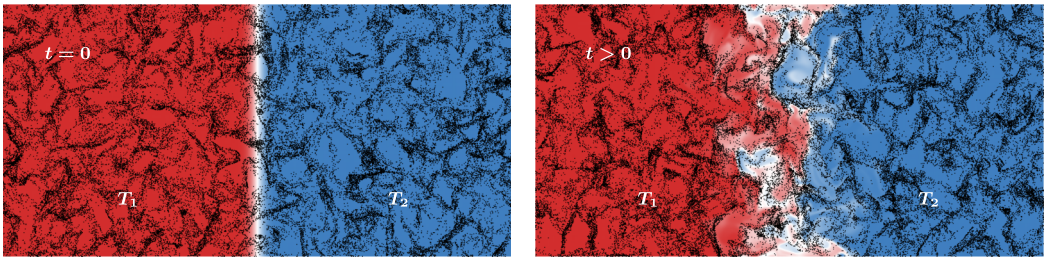


FIG. 1. Schematic of the time-developing turbulent thermal mixing layer. Two initially homothermal regions at different temperatures are advected by a homogeneous and isotropic velocity field. A temporal mixing layer develops between them, while inertial particles (black dots) are advected, cluster in intermittent regions, and exchange heat with the fluid.

(i) Phase-space analysis of particle dynamics, based on the transport equation for the probability density function (PDF) of particle state variables (position, velocity, temperature). Exploiting homogeneity in directions normal to the mean gradient, we can analyze the PDF in a reduced-order space, whose dimensions allow a tractable form that can be visualized and compared with DNS data, revealing the most relevant structures in fluid-particle interaction and the possibility of a self-similar stage of evolution [20]; (ii) integral analysis of total enthalpy, by formulating a moment of total enthalpy integral (MTEI) for the coupled fluid-particle system. Building on recent developments in integral methods for turbulent boundary layers [21–24], this approach quantifies the contributions of turbulent convection and particle transport to heat transfer across the mixing layer.

This dual framework allows us to provide both local (PDF-based) and global (MTEI-based) perspectives on fluid-particle thermal coupling. It also enables a systematic evaluation of whether self-similar growth regimes emerge in the presence of particle inertia and thermal inertia, which introduce additional timescales and may disrupt classical self-similarity. Self-similarity is a common organizing principle in turbulence, emphasized in classic treatments such as Townsend [25], and observed in a variety of turbulent flows [26,27]. In scalar mixing layers, self-similar regimes have been identified in the absence of particles [16]. However, inertial particles introduce new mechanisms and timescales, making the onset and character of self-similarity uncertain. Our analysis does not assume self-similarity, but provides criteria for its occurrence and a framework for quantifying deviations when it fails. The results presented here, therefore, extend the theory of turbulent scalar transport to particle-laden flows with inhomogeneous and evolving temperature fields, offering a foundation for more complex and applied studies of particle-heat coupling in environmental and engineering systems.

II. FORMULATION

A. Flow description and physical model

We investigate the fluid-particle thermal interaction in a simple thermal mixing layer generated by the advection of a sharp temperature interface separating two homothermal regions in a turbulent flow. In this situation, the interaction between two unbounded fluid regions at uniform temperatures T_1 and T_2 in a homogeneous and isotropic velocity field with zero mean velocity generates an intermittent thermal layer [17]. A sketch of the system is shown in Fig. 1. The flow is assumed to be incompressible, so that the temperature field acts as a passive scalar field, advected by the flow. As in [17], we indicate with x_3 the inhomogeneous direction, so that the region at temperature T_1 is initially defined by $x_3 < 0$, and the region at temperature T_2 is initially defined by $x_3 > 0$.

At the same time, the flow is seeded by a set of small, identical inertial particles with a finite thermal capacity. The state of a small spherical heavy particle moving in a fluid and thermally interacting with the fluid is given by its position $\boldsymbol{X}_p$, its velocity $\boldsymbol{V}_p$, and its temperature Θ_p. Their

dynamics, in the limit of radius much smaller than any flow scale and density much higher than the fluid, i.e., $\rho_p/\rho_f \gg 1$ and $(\rho_p c_{pp})/(\rho_f c_{pf}) \gg 1$, where ρ_p and ρ_f are the particle and fluid density, and c_{pp} and c_{pf} are the particle and fluid specific heat at constant pressure, obey the following equations:

$$\frac{\mathrm{d}}{\mathrm{d}t}\begin{Bmatrix} \boldsymbol{X}_p(t) \\ \boldsymbol{V}_p(t) \\ \Theta_p(t) \end{Bmatrix} = \begin{bmatrix} 0 & 1 & 0 \\ 0 & -1/\tau_v & 0 \\ 0 & 0 & -1/\tau_\vartheta \end{bmatrix} \begin{Bmatrix} \boldsymbol{X}_p(t) \\ \boldsymbol{V}_p(t) \\ \Theta_p(t) \end{Bmatrix} + \begin{bmatrix} 0 \\ (1/\tau_v)\boldsymbol{u}(t, \boldsymbol{X}_p(t)) \\ (1/\tau_\vartheta)T(t, \boldsymbol{X}_p(t)) \end{bmatrix}. \tag{1}$$

Equations (1) are a simplified version of the Maxey-Riley-Gatignol (MRG) equation, which is considered the theoretical foundation of almost all point-particle Eulerian-Lagrangian approaches. The MRG equation was proposed by Maxey and Riley [28], and independently by Gatignol [29] in 1983. Note that, in general, for finite-size particles, like particles comparable to or larger than the Kolmogorov length scale, the MRG equation's applicability is limited, and additional corrections or alternative models are needed to account for size effects. Although the MRG equation is valid for low-particle Reynolds number ($\mathrm{Re}_p = 2R|\boldsymbol{u}(t, \boldsymbol{X}_p) - \boldsymbol{V}_p|/\nu \ll 1$), it can take into account the effects of finite particle size through the Faxén correction terms, which are a function of Re_p [29]. Homann and Béc [30] showed that the effect of these correction terms is significant for larger particles, but negligible if the particle diameter is equal to the Kolmogorov size or smaller. In our study, the linear model is used under which the nonlinear correction is not needed due to the very low Re_p. Thus, we use a simplified model for the point-like particles in the Stokesian regime ($\mathrm{Re}_p \ll 1$), and without considering the finite-size effect ($R/\eta \ll 1$) and Faxén correction. Moreover, in the limit for $\rho_p/\rho_f \gg 1$, the dominating term in the momentum equation is the Stokes drag, while the Basset, added mass, and pressure gradient forces become negligible [31]. Analogously, under the same conditions, the dominating term in the particle temperature equation is the quasisteady diffusive heat transfer. On the contrary, for light particles, especially neutrally buoyant particles such as bubbles suspended in a denser liquid where the particle density is lower than the fluid density, the other forces, as well as the nonlinear drag correction, cannot be neglected. Interparticle interaction forces, e.g., collision and lubrication forces, are not included in our model, and due to the scale of the smallest particle in this work, Brownian effects are also disregarded [32]. In our study, the particle exchanges heat with the surrounding fluid solely through convection. For a solid particle model, where the particle's mass remains constant throughout the process, latent heat is not included in the enthalpy equation. However, in other scenarios, additional heat transfer mechanisms (such as radiative heat transfer) or heat sources/sinks (such as vaporization enthalpy) may be incorporated into the enthalpy equation. Moreover, conductive heat transfer within the particle is neglected due to the small particle radius. For particles of size $\sim\mathcal{O}(10^{-6})$ m, the Biot number, defined as $\mathrm{Bi} = hR/\lambda_p$ (where h is the convective heat transfer coefficient, λ_p is the particle thermal conductivity, and R is the particle radius), is much smaller than one ($\mathrm{Bi} \ll 1$), indicating that the particle temperature can be considered uniform. Neglecting conduction is justified under the assumption of a finite heat capacity (lumped-capacitance model) because convection is significantly more effective than conduction in this size range. In the particle temperature equation, the disturbances to the local fluid temperature field caused by the particles are not considered. Thus, both Eulerian and Lagrangian equations use undisturbed quantities in this study. Although actual temperature fields would account for both disturbed and undisturbed components, this assumption is justified for the range of our parameters. The statistical moments of the temperature field gradient, including both disturbed and undisturbed fields, have been analyzed by Carbone *et al.* [2]. They showed that, in the valid range of the point-particle approach, there exists a significant scale separation between the particle radius and the Kolmogorov microscale; therefore, an analytical solution for the temperature field can be derived. Carbone *et al.* [2] also addressed the validity of the assumption that particle perturbations can be neglected in the point-particle model. They demonstrated that the margin of error introduced by this assumption is at most about 15% even for large particles with $\mathrm{St} = 3$. This supports our decision to disregard particle-induced disturbances in the fluid temperature field.

Horwitz *et al*., later in [33], showed that in this limit ($R/\eta \ll 1$), the undisturbed temperature and the interpolated temperature at the particle position are nearly identical. In that work, they used thermal energy dissipation as the verifiability measure to support the arguments in [34] concerning the use of symmetric stencils for interpolating and projecting fluid quantities. Here, τ_v and τ_ϑ are the momentum and thermal relaxation times, defined as

$$\tau_u = \frac{2}{9}\frac{\rho_p}{\rho_f}\frac{R^2}{\nu}, \quad \tau_\vartheta = \frac{1}{3}\frac{\rho_p c_{pp}}{\rho_f c_{pf}}\frac{R^2}{\kappa}, \tag{2}$$

where R is the particle radius, ν the kinematic viscosity of the fluid, and κ the thermal diffusivity of the flow. Variables $\boldsymbol{u}(t, \boldsymbol{X}_p)$ and $T(t, \boldsymbol{X}_p)$ are fluid velocity and temperature at particle position, which are solutions of the Navier-Stokes equations,

$$\nabla \cdot \boldsymbol{u} = 0, \tag{3}$$

$$\frac{\partial \boldsymbol{u}}{\partial t} + \boldsymbol{u} \cdot \nabla \boldsymbol{u} = -\frac{1}{\rho_f}\nabla p + \nu \nabla^2 \boldsymbol{u} + \boldsymbol{f}_u, \tag{4}$$

$$\frac{\partial T}{\partial t} + \boldsymbol{u} \cdot \nabla T = \kappa \nabla^2 T + \frac{1}{\rho_f c_{pf}} C_T, \tag{5}$$

where p is the pressure, $\boldsymbol{f}_u$ an external forcing term to keep the velocity field statistically steady, and C_T the particle thermal feedback on the fluid, i.e., the heat transfer from the particles to the fluid phase per unit time and unit volume, which is given by

$$C_T(t, \boldsymbol{x}) = -\frac{4}{3}\pi R^3 \rho_p c_{pp} \sum_{p=1}^{N_p} \frac{\mathrm{d}\Theta_p(t)}{\mathrm{d}t} \delta[\boldsymbol{x} - \boldsymbol{X}_p(t)].$$

This last term, added on the right-hand side of the fluid temperature equation (5), acts as a small-scale source term [2]. In this way, we are considering a two-way thermal coupling between fluid and particles, but only a one-way momentum coupling between particles and fluid. This is appropriate for low volume fractions, or even at moderate volume fractions, approximately up to 10^{-3}, where two-way momentum coupling cannot be neglected, momentum feedback has been shown to have only a minor effect on particle temperature statistics in free flows [2,35], and therefore it is often neglected [1]. When the flow is turbulent, fluid velocity and temperature in (1) act as stochastic forcing for the particle, leading to particle random motion. We use a particle volume fraction of $\varphi = 4 \times 10^{-4}$ in all simulations. This value is sufficient for two-way thermal and momentum coupling between particles and fluid to be significant, yet low enough to neglect interparticle collisions and interactions, which become notable at volumes greater than 10^{-3}. Moreover, the impact of particle collisions has been reported in [35,36] and suggested to be minor in this range of volume fraction, especially on thermal fields, which is the aim of this study. Although two-way coupling is appropriate for this volume fraction [37], the interaction between convective heat transfer and particles already introduces substantial complexity, so we exclude particle momentum feedback, which has been found to play only a minor role in homogeneous flows [2,38,39].

B. Numerical method and simulation setup

A DNS solves the Navier-Stokes equations together with the Lagrangian tracking of point particles, Eq. (1). These DNSs [17] solve the flow within a parallelepiped domain with dimensions L in the homogeneous directions x_1 and x_2, and $2L$ in the thermally inhomogeneous direction $x_3 = x$. Temperature is initialized by setting it equal to T_1 in the half-domain where $x_3 < 0$ and to T_2 in the half-domain where $x_3 > 0$, while a statistically steady homogeneous and isotropic velocity field is maintained by a forcing through a body force $\boldsymbol{f}_u$, which imposes a constant energy injection rate of ε. The governing equations are solved in dimensionless form, normalizing them

TABLE I. Dimensionless flow parameters.

Taylor microscale Reynolds number	Re_λ	56
Prandtl number	Pr	0.71
mean turbulent kinetic energy dissipation rate	ε	0.25
Forced wave number	k_f	5
Kolmogorov length scale	η	0.0153
Kolmogorov timescale	τ_η	0.098
Taylor microscale	λ	0.226
Integral length scale	ℓ	0.40
Root mean square of velocity fluctuations	u'	0.59
Resolution	$\Delta x/\eta$	1.6
Grid size (after dealiasing)	$N_1 = N_2$	256
	N_3	512
Particle volume fraction	φ	4×10^{-4}
Density ratio	ρ_p/ρ_f	10^3
Stokes number ratio	$\mathrm{St}_\vartheta/\mathrm{St}$	4.43
Stokes number	St	0.2; 0.3; 0.5; 0.7; 0.8; 0.9; 1; 1.2; 1.5; 2; 2.5; 3; 4

by using the size of the domain in the homogeneous direction, $L_0 = L/(2\pi)$, as a reference length, a reference velocity $U_0 = (4\varepsilon L_0)^{1/3}$ deduced from the imposed mean kinetic energy dissipation rate ε through the body force (see [2]), and the temperature difference $T_1 - T_2$. Periodic boundary conditions are applied to all directions to the velocity field and the temperature field, after it has been decomposed as

$$T(t, \boldsymbol{x}) = \frac{T_1 + T_2}{2} + \frac{T_2 - T_1}{2L} x_3 + T_*(t, \boldsymbol{x}). \tag{6}$$

The problem is put in dimensionless form using the above-mentioned reference scales (see Appendix) and is discretized in space by means of a Fourier-Galërkin method, and integrated in time with a second-order exponential Runge-Kutta integrator. Interpolation of fluid velocity and temperature at particle positions is carried out using a recently developed numerical method [3,40], which relies on inverse and forward non-uniform fast Fourier transforms combined with a fourth-order B-spline basis. All data we present correspond to a single Taylor microscale Reynolds number, $\mathrm{Re}_\lambda = 56$, simulated with $256^2 \times 512$ Fourier modes after dealiasing, which ensures that $k_{\max}\eta \simeq 1.94$. Particle-to-fluid density ratio ρ_p/ρ_f has been kept equal to 10^3, and particle-to-fluid specific heat ratio c_{pp}/c_{pf} has been set equal to 4.16, which is representative of water droplets in air. This implies that the ratio between the thermal Stokes number and the Stokes number, i.e., the ratio of the relaxation times, is equal to 4.43. Particles with different Stokes numbers are obtained by changing their radius. Accordingly, particle number ranges from 2.71×10^6 ($\mathrm{St} = 4$) to 2.43×10^7 ($\mathrm{St} = 0.2$) in order to maintain a constant volume fraction $\varphi = 4 \times 10^{-4}$. All relevant dimensionless parameters are in Table I. Further details on these simulations can be found in [17].

III. PHASE SPACE ANALYSIS

A. Single particle probability density function

In a turbulent flow, the particles are subjected to stochastic forcing by turbulent eddies, leading to random particle motions. The probability density function (PDF) of finding a single particle with a state $\boldsymbol{Z} = (\boldsymbol{X}_p, \boldsymbol{V}_p, \Theta_p)$ is $f_{f.g}(t, \boldsymbol{x}_p, \boldsymbol{v}_p, \vartheta_p) = \delta[\boldsymbol{x}_p - \boldsymbol{X}_p(t)]\delta[\boldsymbol{v}_p - \boldsymbol{V}_p(t)]\delta[\vartheta_p - \Theta_p(t)]$, which,

averaged over all the possible realizations, gives the coarse-grained PDF f:

$$f(t, \boldsymbol{x}_p, \boldsymbol{v}_p, \vartheta_p) = \langle f_{f.g}(t, \boldsymbol{x}_p, \boldsymbol{v}_p, \vartheta_p)\rangle = \int \mathrm{d}\boldsymbol{x}_p \mathrm{d}\boldsymbol{v}_p \mathrm{d}\vartheta_p \delta[\boldsymbol{x}_p - \boldsymbol{X}_p(t)]\delta[\boldsymbol{v}_p - \boldsymbol{V}_p(t)]\delta[\vartheta_p - \Theta_p(t)]. \tag{7}$$

The evolution equation for f, for noncolliding particles, is obtained from the integration of the time derivative of the fine-grained PDF, when Eq. (1) is used, leading to

$$\frac{\partial f(t, \boldsymbol{x}_p, \boldsymbol{v}_p, \vartheta_p)}{\partial t} + \frac{\partial}{\partial \boldsymbol{x}_p}[f(t, \boldsymbol{x}_p, \boldsymbol{v}_p, \vartheta_p)\langle \boldsymbol{V}_p | \boldsymbol{x}_p, \boldsymbol{v}_p, \vartheta_p\rangle] + \frac{\partial}{\partial \boldsymbol{v}_p}[f(t, \boldsymbol{x}_p, \boldsymbol{v}_p, \vartheta_p)\langle \boldsymbol{A}_p | \boldsymbol{x}_p, \boldsymbol{v}_p, \vartheta_p\rangle]$$
$$+ \frac{\partial}{\partial \vartheta_p}[f(t, \boldsymbol{x}_p, \boldsymbol{v}_p, \vartheta_p)\langle \dot{\Theta}_p | \boldsymbol{x}_p, \boldsymbol{v}_p, \vartheta_p\rangle] = 0, \tag{8}$$

where $\boldsymbol{A}_p = \mathrm{d}\boldsymbol{V}_p/\mathrm{d}t$ and $\dot{\Theta} = \mathrm{d}\Theta/\mathrm{d}t$ are given by Eq. (1). Since short-range particle-particle interactions (e.g., electrostatic or direct hydrodynamic interactions) are not considered, the single-particle PDF equation can be used to describe their collective dynamics [32]. In the absence of collisions, particles are correlated by the interaction with the fluid phase.

The Lagrangian PDF, Eq. (8), includes some unclosed terms, the conditional averages of velocity, acceleration, and temperature derivative, since they involve fluid fluctuations. Note that this PDF is derived under the assumptions that the process is Markovian and that initial states are equal to zero. An Eulerian form of this PDF can be obtained by integrating over all particles that pass through a given state $(\boldsymbol{x}, \boldsymbol{v}, \vartheta)$ at time t,

$$f^E(t, \boldsymbol{x}, \boldsymbol{v}, \vartheta) = \int \mathrm{d}\boldsymbol{x}_p \mathrm{d}\boldsymbol{v}_p \mathrm{d}\vartheta_p f(t, \boldsymbol{x}_p, \boldsymbol{v}_p, \vartheta_p)\delta[\boldsymbol{x} - \boldsymbol{x}_p(t)]\delta[\boldsymbol{v} - \boldsymbol{v}_p(t)]\delta[\vartheta - \vartheta_p(t)]. \tag{9}$$

This integral effectively transforms the Lagrangian description into an Eulerian description using Dirac delta functions to enforce the condition that the particle's phase space coordinates match the Eulerian coordinates [41]. Since the Lagrangian PDF, f, is already a function of state variable $(\boldsymbol{x}_p, \boldsymbol{v}_p, \vartheta_p)$, and the delta function ensures we are evaluating at $(\boldsymbol{x}, \boldsymbol{v}, \vartheta)$, therefore, we get

$$f^E(t, \boldsymbol{x}, \boldsymbol{v}, \vartheta) = f(t, \boldsymbol{x}_p = \boldsymbol{x}, \boldsymbol{v}_p = \boldsymbol{v}, \vartheta_p = \vartheta). \tag{10}$$

In the Eulerian framework, we are concerned with the density of particles at fixed spatial coordinates, characterized by specific velocities and temperatures, and averaged over all particles in the domain. In contrast, the Lagrangian description focuses on the instantaneous states of individual particles as they move along their trajectories, represented by the state variables $(\boldsymbol{X}_p(t), \boldsymbol{V}_p(t), \Theta_p(t))$. The Eulerian state variables $(\boldsymbol{x}, \boldsymbol{v}, \vartheta)$, on the other hand, describe the state of the system at fixed spatial points at a specific time t.

In general, Eq. (8) is formulated in a seven-dimensional space $\boldsymbol{Z}$. In the present specific problem, the flow field which drives particle motions is characterized by homogeneous and isotropic velocity fluctuations and a temperature which is statistically homogeneous in two directions, x_1 and x_2, and whose PDF is a function of $x_3 = x$ and t only, so that f does not depend on (x_1, x_2). We can further integrate f over (v_1, v_2) to reduce the dimensionality of the problem to three and obtain a reduced PDF f_*,

$$f_*(t, x_p, v_p, \vartheta_p) = \int_{\Sigma(x_p, v_p)} f(t, \boldsymbol{x}_p, \boldsymbol{v}_p, \vartheta_p)\mathrm{d}v_{p,1}\mathrm{d}v_{p,2}, \tag{11}$$

where $\Sigma(x_p, v_p) = \{(t, \boldsymbol{x}_p, \boldsymbol{v}_p, \vartheta) : x_{p,3} = x_p,\ v_{p,3} = v_p\}$. which describes the probability to find, at time t, a particle in a plane x_3 normal to the inhomogeneous direction, with velocity component v_3 along the inhomogeneous direction x_3 and temperature θ_p. By integrating Eq. (8), taking advantage of the fact that the velocity field is homogeneous and isotropic, the reduced probability density

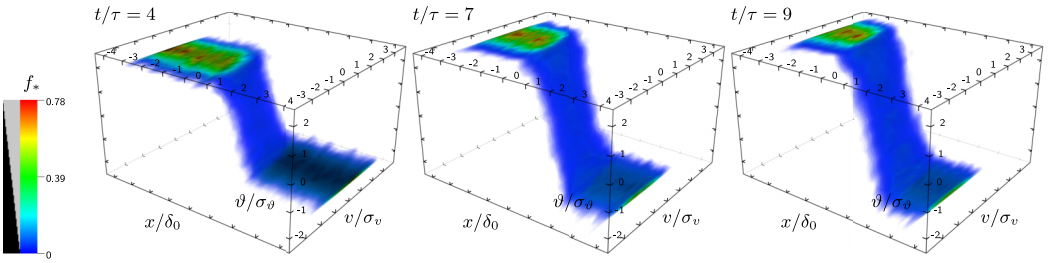


FIG. 2. Three-dimensional rendering of the reduced single-particle PDF, f_*, at St = 1.0 at $t/\tau = 4$, 7, and 9. Position x, velocity v, and temperature ϑ have been normalized with the mixing layer thickness δ, the velocity standard deviation, and the temperature standard deviation in the middle section.

function obeys the following equation:

$$\frac{\partial f_*(t, x_p, v_p, \vartheta_p)}{\partial t} + \frac{\partial}{\partial x_p}[f_*(t, x_p, v_p, \vartheta_p)\langle V_p|x_p, v_p, \vartheta_p\rangle] + \frac{\partial}{\partial \vartheta_p}[f_*(t, x_p, v_p, \vartheta_p)\langle \dot{\Theta}_p|x_p, v_p, \vartheta_p\rangle] = 0, \tag{12}$$

where, for the sake of clarity, subscript 3 will be omitted from this point onward.

Equation (12) can be solved only after the unclosed terms are modelled. As it is customary in many physical problems concerning phase-space analysis, e.g., astrophysics and accelerator physics [20], we employ data from DNS to analyze the PDF in a reduced ordered phase space, whose dimensions are determined by particle state variables X_p, V_p, and Θ_p.

B. Results

We deduce the reduced PDF of the particles, f_*, and all relevant unclosed terms from DNS data. In particular, we focus on the most significant moment of the PDF transport equation (12), i.e., the conditional average of the particle temperature time derivative $\langle \dot{\Theta}_p|x_p, v_p, \vartheta_p\rangle$. More precisely, we aim to further analyze the PDF behavior in phase space via three-dimensional and two-dimensional visual inspections of the PDF obtained in Sec. III A. We consider DNS at a Taylor microscale Reynolds number equal to 56, varying the Stokes number $\mathrm{St} = \tau_v/\tau_\eta$, the ratio between the momentum relaxation time τ_v equation (2) and the timescale of the smallest turbulent eddies, and the Kolmogorov timescale $\tau_\eta = (\nu/\epsilon)^{1/4}$, from 0.2 to 6, while keeping the ratio between thermal relaxation times τ_ϑ/τ_v equal to 4.43.

An example of the three-dimensional structure of the reduced particle PDF $f_*(t, x, v, \theta)$ is shown in Fig. 2 for particles with a Stokes number equal to 1 at dimensionless times t/τ equal to 4, 7, and 9. Here, $\tau = \ell/u'$ is the turbulence eddy turnover time, with u' the root mean square of fluid velocity fluctuations and ℓ their correlation length. Function f_* is obtained through a bin count, where the bin size has been carefully selected to strike a balance between adequate resolution in phase space and data sampling. The velocity and temperature fluctuations have been normalized with their respective standard deviations, in the whole domain for the velocity field, which is statistically homogeneous and steady, taken at $x = 0$ for the temperature field, which is inhomogeneous and unsteady. The position x has been rescaled with a conventional thickness δ_0 based on the gradient of the mean fluid temperature, $\delta_0 = (T_1 - T_2)[\partial\langle T\rangle/\partial x(t, 0)]^{-1}$, as in [17]. In the two homogeneous regions, particles are all concentrated around the uniform temperatures of the two zones. As the time progresses, a mixing zone around $x = 0$ develops and gradually grows, expanding toward the homogeneous regions. This produces a link between the nonzero regions of f_*, as particles, advected through this layer by turbulence and interacting thermally with a nonhomothermal fluid, cool or warm.

After an initial transient, f_* appears to approach a time-invariant shape when position, velocity, and temperature are properly rescaled. In this situation, particle fluctuations are determined only by the local standard deviations of velocity and temperature.

The evolution of f_* in this zone is shown in Figs. 3, 4, and 5, which present the time evolution of f_* in the two-dimensional section $x = 0$ for particles with different Stokes numbers, from 0.2 to 4. Dark colors on the maps indicate lower values (black indicates a zero value of f_*) and brighter colors represent the higher values. The region with nonzero probability forms an elliptical-like structure, stretching diagonally, which remains almost invariant, aligned with the bisector of the first and third quadrants when v and ϑ are rescaled by the respective standard deviations at $x = 0$, while x has been rescaled using a conventional scale δ_0 of the thermally inhomogeneous layer [see [17], Eq. (15)]. This shape can be easily interpreted through a simple quadrant method. Mean temperature decreases with x, and there is a net heat flux in the positive direction. The mean dimensionless fluid temperature is zero at $x = 0$. In physical space, particles with a positive velocity v come from regions with a higher mean temperature, so they tend to be warmer than the surrounding fluid ($\vartheta > 0$) and, on average, are cooled ($\dot{\Theta}_p = (T - \vartheta)/\tau_\vartheta < 0$), while particles moving in the opposite direction ($v < 0$) come from regions with a lower mean temperature, so that they tend to be colder than the surrounding fluid ($\vartheta < 0$) and therefore, on average, are warmed by the interaction with the fluid. This is consistent with a positive temperature-velocity correlation, which is expected as heat is transferred toward the positive direction of x. This produces the skewed distribution that can be observed. Moreover, the white line superimposed on the contours represents the states where the mean particle temperature time derivative $\langle \dot{\Theta}_p | x, v, \vartheta \rangle$ is zero, and separates the states in which particles are, on average, cooled (above the line) from the states in which particles are, on average, warmed (below the line). It is an almost straight line with a constant slope, so that most of the first quadrant shows a negative $\dot{\Theta}_p$, and most of the third quadrant shows a positive $\dot{\Theta}_p$.

As time evolves, it is possible to identify an initial stage of evolution, which lasts around four fluid time-scales during which particles are moved by turbulence in a thermally inhomogeneous region and begin to interact with the surrounding fluid (so that the two blobs at dimensionless temperature ± 1 develop into a narrow worm connecting those temperatures), and a later stage, where this joint PDF creates an elliptical-like structure aligned along the bisector, which remains almost time invariant. The particle PDF relaxes toward a sort of dynamical equilibrium determined by the local mean fluid temperature gradient, which, as time evolves, changes more and more slowly. This stage should be followed by a final stage of evolution, where the fluid temperature field becomes almost homogeneous, and thus the correlation between velocity and temperature vanishes

The Stokes number determines the intensity of the correlation and, to a lesser extent, the duration of the different phases, as a larger Stokes number implies a larger particle inertia and thermal inertia, which delays the interphase momentum and heat transfer.

In this plane, it is also possible to appreciate the general symmetry $f_*(t, -x, -v, -(\vartheta - \langle T \rangle)) = f_*(t, x, v, \vartheta - \langle T \rangle)$ of the solution of (12), since for $x = 0$ and (dimensionless) $\langle T \rangle = 0$, it implies $f_*(t, 0, -v, -\vartheta) = f_*(t, x, v, \vartheta)$.

A similar behavior seems to be present even at $x \neq 0$, as shown in Fig. 5, even if delayed; i.e., the relaxation of the PDF into an oval shape aligned along the bisector of the first and third quadrants is delayed. Indeed, temperature fluctuations are generated at $x = 0$ by turbulence and then spread by a sort of turbulent self-diffusion, so that a time proportional to x^2 is required before temperature fluctuations reach any given position x. Anyway, after it occurs, the local particle PDF at a fixed x tends to be determined as well only by the standard deviation of the velocity and temperature once the fluid temperature varies randomly. However, since temperature is constrained between T_1 and T_2, particle variances are lower than at the plane at $x = 0$, and the slope of both the elliptical structure and the separating line with zero mean temperature changes with x.

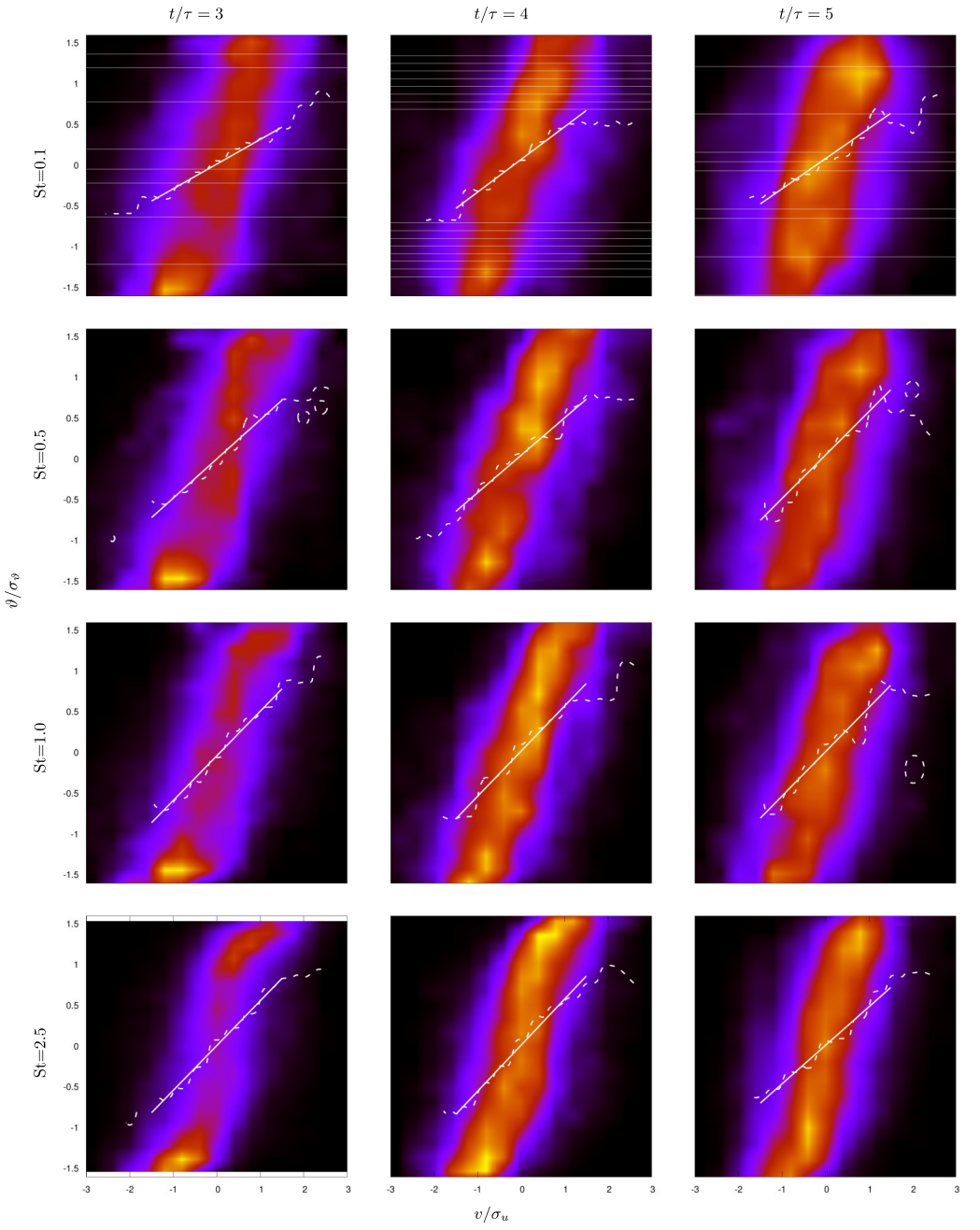


FIG. 3. Time evolution of a slice of reduced single-particle PDF f_* in the central plane $x = 0$ for different St at $\mathrm{Re}_\lambda = 56$ and when $\mathrm{St}_\vartheta/\mathrm{St} = 4.43$. The dark color indicates lower values, and the brighter colors indicate higher values. Velocity and temperature have been normalized with their standard deviations. The continuous white line indicates the state where the mean particle temperature time derivative $\langle \dot{\Theta}_p | x, v, \vartheta \rangle$ is zero, and the dashed lines indicate the states where the particle temperature time derivatives are equal to $\pm 0.2\sigma_\vartheta/\tau_\vartheta$.

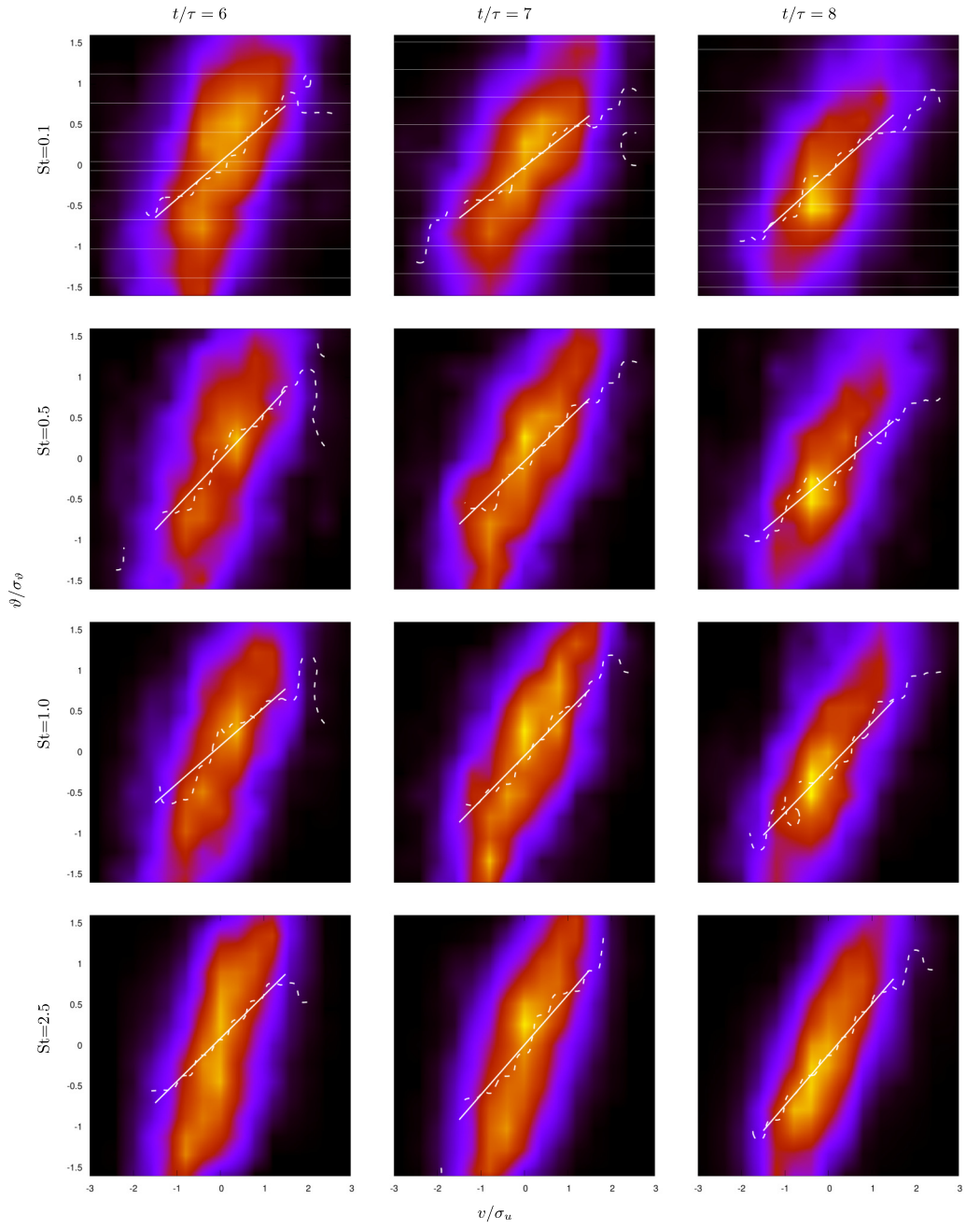


FIG. 4. Same data as previous figure, at later times, see its caption.

IV. SELF-SIMILARITY ANALYSIS OF FIRST-ORDER MOMENT OF TOTAL ENTHALPY INTEGRAL EQUATIONS

As discussed in Sec. III, the dynamics of the particles appear to lead toward a stage where f_* is determined by the local variance of velocity and temperature, and by the rescaled position along x,

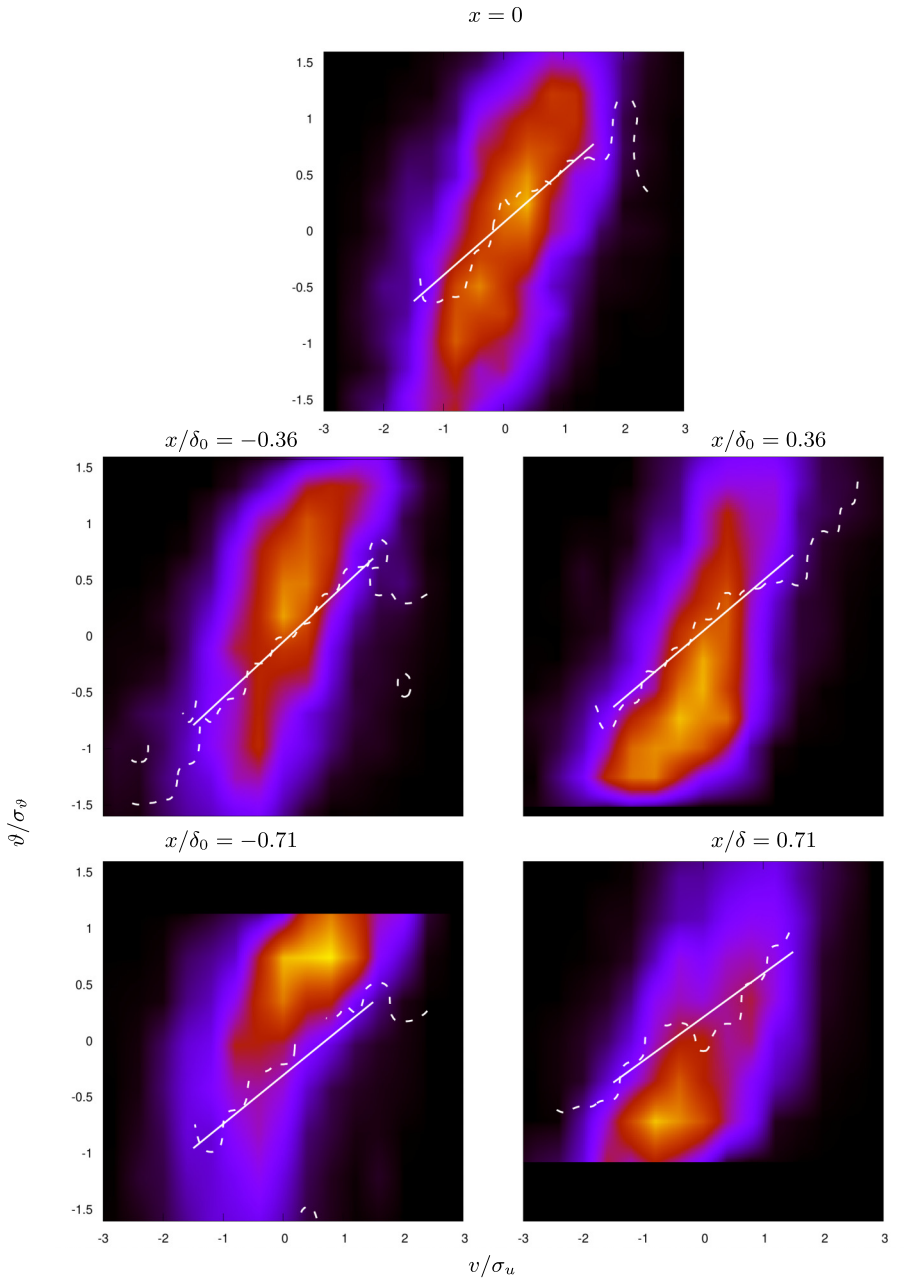


FIG. 5. Same data as the previous figure, at a fixed time $t/\tau = 6$, St $= 1$ and different planes (symmetric planes around $x = 0$).

which implies the mean temperature. This implies that the behavior of f_* tends to be self-similar and, as a consequence, all its moments would also become self-similar.

In this section, we consider the evolution of the moments of f_*, in particular, the moments that are associated with the enthalpy of the system, i.e., the temperature ones. This also leads to a more manageable problem with a lower dimensionality. Multiplication of Eq. (12) by ϑ and integration

over all the temperatures leads to

$$\frac{\partial\langle\vartheta\rangle}{\partial t}+\frac{\partial\langle v\vartheta\rangle}{\partial x}=\frac{1}{\tau_\vartheta}[\langle T\rangle-\langle\vartheta\rangle], \tag{13}$$

where $\langle\vartheta\rangle=\int\vartheta f_*\,\mathrm{d}\vartheta\,\mathrm{d}v$, and the temperature derivative has been expressed using (1). The average mean fluid temperature $\langle T\rangle$ can be obtained from the advection-diffusion equation for fluid temperature fluctuations. Its statistical average, under the assumption of isotropic velocity fluctuations, leads to

$$\frac{\partial\langle T\rangle}{\partial t}=\kappa\frac{\partial^2\langle T\rangle}{\partial x^2}-\frac{\partial\langle uT\rangle}{\partial x}-\varphi_\vartheta\frac{\langle T\rangle-\langle\vartheta\rangle}{\tau_\vartheta}, \tag{14}$$

where $\varphi_\vartheta=\varphi(\rho_p c_{pp})/(\rho_f c_{pf})$, and is the ratio between the thermal capacity of the particle phase and the thermal capacity of the carrier flow. The last term in Eq. (14) derives from the particle thermal feedback on the fluid phase [17]. By summing Eqs. (13) and (14), we obtain a balance equation for the total enthalpy of the system, and the sum of the fluid and particle enthalpy, $\rho_f c_{pf}(\langle T\rangle+\varphi_\vartheta\langle\vartheta\rangle)$:

$$\frac{\partial}{\partial t}(\langle T\rangle+\varphi_\vartheta\langle\vartheta\rangle)+\frac{\partial}{\partial x}(\langle uT\rangle+\varphi_\vartheta\langle v\vartheta\rangle)=\kappa\frac{\partial^2\langle T\rangle}{\partial x^2}. \tag{15}$$

Given the symmetry of the problem, i.e., $x\to -x$ and $T-T_m\to -(T-T_m)$ leave the problem unchanged, we can consider only the region $x>0$. If we subtract the temperature T_2 from both T and ϑ, we have an equation for the variation of the enthalpy from the initial condition. In order to reduce the numerical noise due to a limited statistical sample, we derive integral quantities. We can integrate this equation along x in the whole half domain, obtaining

$$\frac{\mathrm{d}}{\mathrm{d}t}\left[\int_0^\infty(\langle T\rangle-T_2)\mathrm{d}x+\varphi_\vartheta\int_0^\infty(\langle\vartheta\rangle-T_2)\mathrm{d}x\right]=\langle u'T'\rangle(t,0)+\varphi_\vartheta\langle v'\vartheta'\rangle(t,0)-\kappa\frac{\partial T}{\partial x}(t,0). \tag{16}$$

From this equation, it is possible to define a temperature thickness, which gives a measure of the broadening of the thermal interaction layer between the two regions, analogous to the momentum thickness of a boundary layer, but based on the difference in the total enthalpy of the system, which is proportional to $\langle T\rangle+\varphi_\vartheta\langle\vartheta\rangle$, with respect to the homogeneous region,

$$\delta(t)=\frac{2}{1+\varphi_\vartheta}\int_0^\infty\left[\frac{\langle T\rangle-T_2}{T_1-T_2}+\varphi_\vartheta\frac{\langle\vartheta\rangle-T_2}{T_1-T_2}\right]\mathrm{d}x, \tag{17}$$

so that Eq. (16) can be written as

$$(1+\varphi_\vartheta)\frac{T_1-T_2}{2}\frac{\mathrm{d}}{\mathrm{d}t}\delta=\langle u'T'\rangle(t,0)+\varphi_\vartheta\langle v'\vartheta'\rangle(t,0)-\kappa\frac{\partial T}{\partial x}(t,0). \tag{18}$$

The terms on the right-hand side represent the heat transfer $\langle\dot{q}_x\rangle$ between the two regions, which is given by the sum of three contributions: thermal diffusion (last term), convection by turbulence (first term), and particle motions (middle term). If the thickness δ is used as reference length, the right-hand side of Eq. (18) can then be expressed in terms of Nusselt numbers. Since the overall heat flux is the sum of the mean diffusion in the fluid phase and the transport by fluid fluctuations and particle motion [17,42], we can define the Nusselt number

$$\mathrm{Nu}=\left(\lambda\frac{T_1-T_2}{2\delta(t)}\right)^{-1}\langle\dot{q}_x\rangle(t,0)=\mathrm{Nu}_c+\mathrm{Nu}_p+\mathrm{Nu}_d,$$

where

$$\mathrm{Nu}_c = \left(\kappa \frac{T_1 - T_2}{2\delta(t)}\right)^{-1} \langle u'T' \rangle, \quad \mathrm{Nu}_p = \left(\kappa \frac{T_1 - T_2}{2\delta(t)}\right)^{-1} \varphi_\vartheta \langle v'\vartheta' \rangle(t, 0),$$
$$\mathrm{Nu}_d = \left(\frac{T_1 - T_2}{2\delta(t)}\right)^{-1} \frac{\partial \langle T \rangle(t, 0)}{\partial x},$$

so that (18) can be expressed as

$$(1 + \varphi_\vartheta)\frac{\mathrm{d}}{\mathrm{d}t}\delta = \frac{\kappa}{\delta}(\mathrm{Nu}_c + \mathrm{Nu}_p + \mathrm{Nu}_d). \tag{19}$$

Therefore, knowledge of the temporal evolution of δ is enough to determine the Nusselt numbers. However, this equation alone cannot distinguish the contribution of particles from the contribution of fluid convection and diffusion.

A. Moment of total enthalpy integral

The aim is to cleanly split the heat transfer in a particle-laden turbulent mixing layer into a diffusive Nusselt number, a turbulent correlation contribution, and a particle contribution, for particles with different Stokes numbers. For this reason, we introduce a moment of the enthalpy integral equation to quantify how turbulence and the presence of particles modulate heat flux across the mixing layer. Due to the symmetry $t \to t, x \to -x$, and $T - T_m \to -(T - T_m)$, we can consider only half of the domain. Multiplying (15) by x and integrating over the half domain leads to

$$\frac{\mathrm{d}}{\mathrm{d}t}\int_0^\infty x[(\langle T \rangle - T_2) + \varphi_\vartheta(\langle \vartheta \rangle - T_2)]\mathrm{d}x$$
$$= \kappa \int_0^\infty x \frac{\partial^2 \langle T \rangle}{\partial x^2}\mathrm{d}x - \int_0^\infty x \frac{\partial \langle uT \rangle}{\partial x}\mathrm{d}x - \varphi_\vartheta \int_0^\infty x \frac{\partial \langle v\vartheta \rangle}{\partial x}\mathrm{d}x. \tag{20}$$

Straightforward integration by parts of the integrals on the right-hand side leads to

$$\frac{\mathrm{d}}{\mathrm{d}t}\int_0^\infty x[(\langle T \rangle - T_2) + \varphi_\vartheta(\langle \vartheta \rangle - T_2)]\mathrm{d}x = \kappa \frac{T_2 - T_1}{2} - \int_0^\infty \langle uT \rangle \mathrm{d}x - \varphi_\vartheta \int_0^\infty \langle v\vartheta \rangle \mathrm{d}x, \tag{21}$$

which can be written as

$$\frac{\mathrm{d}}{\mathrm{d}t}(\mathcal{I}_f + \varphi_\vartheta \mathcal{I}_p) = \kappa \frac{T_2 - T_1}{2} + \mathcal{J}_f + \varphi_\vartheta \mathcal{J}_p, \tag{22}$$

where we define

$$\mathcal{I}_f = \int_0^\infty x(\langle T \rangle - T_2)\mathrm{d}x$$
$$\mathcal{I}_p = \int_0^\infty x(\langle \vartheta \rangle - T_2)\mathrm{d}x$$
$$\mathcal{J}_f = \int_0^\infty \langle u'T' \rangle \mathrm{d}x$$
$$\mathcal{J}_p = \int_0^\infty \langle v'\vartheta' \rangle \mathrm{d}x.$$

Integrals $\mathcal{I}_f$ and $\mathcal{I}_p$ are the moments of the fluid and particle mean temperature distributions, while integrals $\mathcal{J}_f$ and $\mathcal{J}_p$ are the convective heat-flux integrals for the fluid and the particles. It is more appropriate to introduce a dimensionless form of the temperature and flux distributions, so that, by

writing

$$\langle T\rangle(t,x) - T_2 = \frac{T_1 - T_2}{2}(1 + \phi_f(t,\eta))$$
$$\langle \vartheta\rangle(t,x) - T_2 = \frac{T_1 - T_2}{2}(1 + \phi_p(t,\eta))$$
$$\langle uT\rangle(t,x) = \kappa\,\mathrm{Pe}\frac{T_1 - T_2}{2}\delta^{-1}\psi_f(t,\eta)$$
$$\langle v\vartheta\rangle(t,x) = \kappa\,\mathrm{Pe}\frac{T_1 - T_2}{2}\delta^{-1}\psi_p(t,\eta),$$

where $\eta = x/\delta$, with δ defined by Eq. (17), and $\mathrm{Pe} = u'\ell/\kappa$ is the Péclet number, based on the flow integral scale ℓ, so that

$$\mathcal{I}_f = \frac{T_1 - T_2}{2}\delta^2\mathcal{I}_f^*,$$
$$\mathcal{I}_p = \frac{T_1 - T_2}{2}\delta^2\mathcal{I}_p^*,$$
$$\mathcal{J}_f = \frac{T_1 - T_2}{2}\kappa\,\mathrm{Pe}\mathcal{J}_f^*,$$
$$\mathcal{J}_p = \frac{T_1 - T_2}{2}\kappa\,\mathrm{Pe}\mathcal{J}_p^*,$$

where

$$\mathcal{I}_f^* = \int_0^\infty \eta(1 + \phi_f(t,\eta))\mathrm{d}\eta,$$
$$\mathcal{I}_p^* = \int_0^\infty \eta(1 + \phi_p(t,\eta))\mathrm{d}\eta,$$
$$\mathcal{J}_f^* = \int_0^\infty \psi_f(t,\eta)\mathrm{d}\eta,$$
$$\mathcal{J}_p^* = \int_0^\infty \psi_p(t,\eta)\mathrm{d}\eta,$$

and Eq. (22) becomes

$$\frac{\mathrm{d}}{\mathrm{d}t}[(\mathcal{I}_f^* + \varphi_\vartheta\mathcal{I}_p^*)\delta^2] = \kappa[1 + \mathrm{Pe}(\mathcal{J}_f^* + \varphi_\vartheta\mathcal{J}_p^*)], \tag{23}$$

which can be integrated, by assuming $\delta(0) = 0$, to give

$$\delta^2 = \kappa(\mathcal{I}_f^* + \varphi_\vartheta\mathcal{I}_p^*)^{-1}\int_0^t [1 + \mathrm{Pe}(\mathcal{J}_f^* + \varphi_\vartheta\mathcal{J}_p^*)]\mathrm{d}t. \tag{24}$$

Since δ is defined by Eq. (17) and is linked to the Nusselt number by Eq. (19), so that the two equations should coincide, the Nusselt number can be expressed in terms of the integrals of temperature moments and fluxes. In fact, Eq. (19) implies that

$$\delta^2(t) = \frac{2\kappa}{1 + \varphi_\vartheta}\int_0^t \mathrm{Nu}\,\mathrm{d}t,$$

so that

$$\int_0^t \mathrm{Nu}\,\mathrm{d}t = \frac{1 + \varphi_\vartheta}{2(\mathcal{I}_f^* + \varphi_\vartheta\mathcal{I}_p^*)}\int_0^t [1 + \mathrm{Pe}(\mathcal{J}_f^* + \varphi_\vartheta\mathcal{J}_p^*)]\mathrm{d}t. \tag{25}$$

Note that the forms of the dimensionless temperature and flux distributions do not imply an assumption of self-similarity, which is achieved only if ϕ_f, ϕ_p, ψ_f, and ψ_p do not depend explicitly on time but only implicitly through δ. In the case that this self-similar behavior is achieved, $\mathcal{I}_f^*$, $\mathcal{I}_p^*$, $\mathcal{J}_f^*$, and $\mathcal{J}_p^*$ are constant, so that (24) reduces to

$$\delta^2 = \kappa \frac{1 + \mathrm{Pe}(\mathcal{J}_f^* + \varphi_\vartheta \mathcal{J}_p^*)}{\mathcal{I}_f^* + \varphi_\vartheta \mathcal{I}_p^*} t, \tag{26}$$

and, as a consequence, the Nusselt number is also constant,

$$\mathrm{Nu} = \frac{1 + \varphi_\vartheta}{2} \frac{1 + \mathrm{Pe}(\mathcal{J}_f^* + \varphi_\vartheta \mathcal{J}_p^*)}{\mathcal{I}_f^* + \varphi_\vartheta \mathcal{I}_p^*}. \tag{27}$$

Self-similarity requires that both $\mathcal{I}_f^* + \varphi_\vartheta \mathcal{I}_p^*$ and $\mathcal{J}_f^* + \varphi_\vartheta \mathcal{J}_p^*$ become time-independent.

This reformulation of the mean enthalpy equation allows us to analyze the contributions of the different particles and the fluid in the growth of the mixed region and, thus, in the overall net heat (enthalpy) flow across the initial temperature discontinuity. The baseline to identify the role of particles is the unseeded flow, i.e., what would be obtained in a one-way coupled regime, because in that situation the fluid motion is independent of the presence of particles and the transport is due only to turbulence, which advects temperature. However, the presence of particles does not limit itself to adding a nonzero thermal capacity through parameter φ_ϑ, because the thermal feedback of the particles modulates fluid fluctuations and, as a consequence, also the fluid phase integrals $\mathcal{I}_f^*$ and $\mathcal{J}_f^*$.

From Eqs. (25) and (27), it is possible to separate the contributions of mean diffusion, convection, and particles. In Eqs. (25) and (27), we have $\mathrm{Nu} = f(\mathcal{I}_f^*, \mathcal{J}_f^*, \mathcal{I}_p^*, \mathcal{J}_p^*, \varphi_\vartheta)$. The contribution of the fluid phase is obtained by setting $\varphi_\vartheta = 0$ in (25), the diffusive one, Nu_d, corresponds to $\mathcal{J}_f^* = 0$, and the rest is the convective contribution Nu_c. The difference $\mathrm{Nu} - (\mathrm{Nu}_d + \mathrm{Nu}_c)$ gives the contribution of the particles Nu_p.

Since we consider the thermal feedback of the particles on the flow, $\mathcal{I}_f^*$ and $\mathcal{J}_f^*$ also depend on the particle concentration, i.e., the particle thermal capacity and the particle Stokes number. The difference between Nu_c in the presence of particles with a given volume fraction and Stokes number and Nu_c in the absence of particles provides an integral measure of the modulation of turbulent transport by particles.

In other terms,

$$\mathrm{Nu}_d = \mathrm{Nu}(\varphi_\vartheta = 0, \mathcal{J}_f^* = 0) = \frac{1}{2\mathcal{I}_f^*}$$

$$\mathrm{Nu}_c = \mathrm{Nu}(\varphi_\vartheta = 0) - \mathrm{Nu}(\varphi_\vartheta = 0, \mathcal{J}_f^* = 0) = \frac{\mathrm{Pe}}{2\mathcal{I}_f^*} \mathcal{J}_f^*$$

$$\begin{aligned} \mathrm{Nu}_p &= \mathrm{Nu} - \mathrm{Nu}_d - \mathrm{Nu}_c = \mathrm{Nu} - \mathrm{Nu}(\varphi_\vartheta = 0) \\ &= \frac{\varphi_\vartheta}{2(\mathcal{I}_f^* + \varphi_\vartheta \mathcal{I}_p^*)} \left[(1 + \mathrm{Pe}\mathcal{J}_f^*) \left(1 + \frac{\mathcal{I}_p^*}{\mathcal{I}_f^*} \right) + (1 + \varphi_\vartheta) \mathrm{Pe}\mathcal{J}_p^* \right], \end{aligned}$$

which corresponds, in integral form, to the definition of the heat transfer as the sum of the mean diffusion, turbulent fluctuation transport, and particle transport [17,43].

B. Numerical results

We use the integral form of the governing equations to analyze data from our DNS. All relevant integrals, including those contributing to the total enthalpy, can be computed from averaged profiles of mean temperature and temperature-velocity correlations for both fluid and particles.

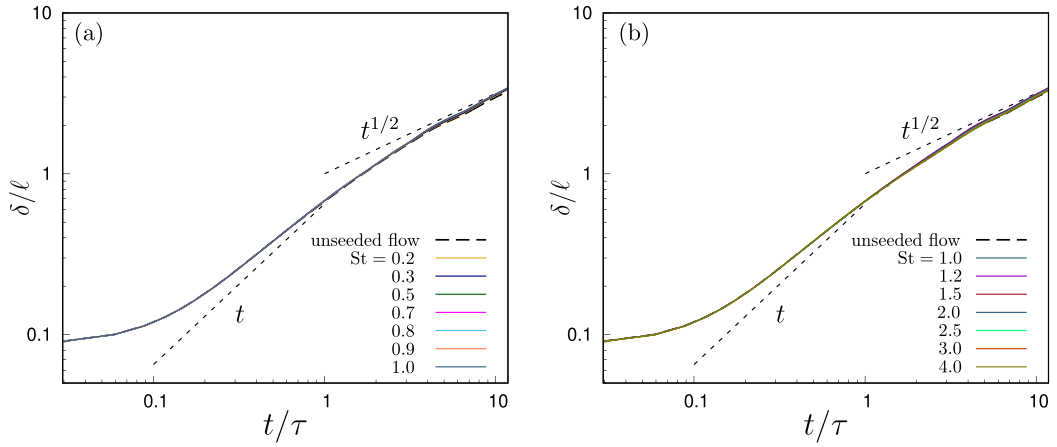


FIG. 6. Temporal growth of δ(t) normalized with integral scale ℓ at $\mathrm{Re}_\lambda = 56$, from the integral form self-similarity analysis of moment of total enthalpy integral in one- and two-way coupling regime: (a) particles with $St \leqslant 1$; (b) particles with $\mathrm{St} \geqslant 1$.

The DNS data are used to measure the enthalpy moment integrals leading to Eq. (25), which defines the Nusselt number. In particular, we consider the dataset from [17,18] for a thermal mixing layer at Taylor Reynolds number $\mathrm{Re}_\lambda = 56$, covering a broad range of Stokes numbers. A fixed ratio $\mathrm{St}_\vartheta/\mathrm{St} = (3/2)(c_{pp}/c_{pf})/\mathrm{Pr}$ is used, determined solely by the thermal properties of the particles. For $c_{pp}/c_{pf} = 4.16$, representative of water droplets in air, this yields $\mathrm{St}_\vartheta/\mathrm{St} = 4.43$.

The evolution of the mixing layer thickness δ, defined in (17), exhibits an asymptotic $t^{1/2}$ growth following an initial transient lasting approximately four eddy turnover times, consistent with [17] (see Fig. 6). The lower value of δ compared to that in [17] arises from a different definition, based here on enthalpy moments rather than the average fluid temperature derivative. This asymptotic growth is indicative of a self-similar regime, as predicted by Eq. (27). In the tracer limit, where the particle and fluid mean temperatures coincide, the mixing layer thickness becomes independent of particle properties. Figure 7 shows the rescaled average temperature and heat fluxes for fluid and particles at $\mathrm{St} = 1$.

The moment integrals of enthalpy provide a compact yet insightful framework for analyzing the contributions to heat transfer. In the self-similar regime, the rescaled temperature moment integrals $\mathcal{I}_f^*$ and $\mathcal{I}_p^*$ remain nearly constant in time (Fig. 8). While these quantities are broadly insensitive to the Stokes number, a weak dependence emerges: the particle moment integral is slightly larger near $\mathrm{St} \sim 1$, coinciding with the peak of particle clustering in the underlying isotropic turbulence. This reflects the enhanced presence of particles in high-strain regions, away from vortical cores where velocity gradients are stronger.

The flux integrals $\mathcal{J}_f$ and $\mathcal{J}_p$ also tend toward stationarity, Figs. 9 and 10, and therefore also the rescaled flux integrals $\mathcal{J}_f^*$ and $\mathcal{J}_p^*$, Fig. 11, although this behavior becomes evident only after the initial transient. In the early evolution, velocity and temperature fields are uncorrelated, particularly for the fluid; this delays the convergence of the flux integral to its self-similar value. This transient is less pronounced in the temperature moment integrals because the initial condition for temperature is imposed with a smooth transition from T_1 to T_2 across a thin layer to avoid Gibbs artifacts. As a consequence, $\mathcal{J}_f$ is initially underestimated while $\mathcal{I}_f$ is overestimated, producing an apparent super-diffusive growth of δ during the early stages as the system adjusts.

Both flux and temperature moment integrals show a nonmonotonic dependence on the Stokes number. The flux integral $\mathcal{J}_p$ attains its maximum near $\mathrm{St} \sim 1$, where particle concentration in high-strain regions is strongest (Fig. 10). This preferential sampling causes particles to traverse areas with elevated velocity-temperature correlations, leading to an enhanced convective heat flux.

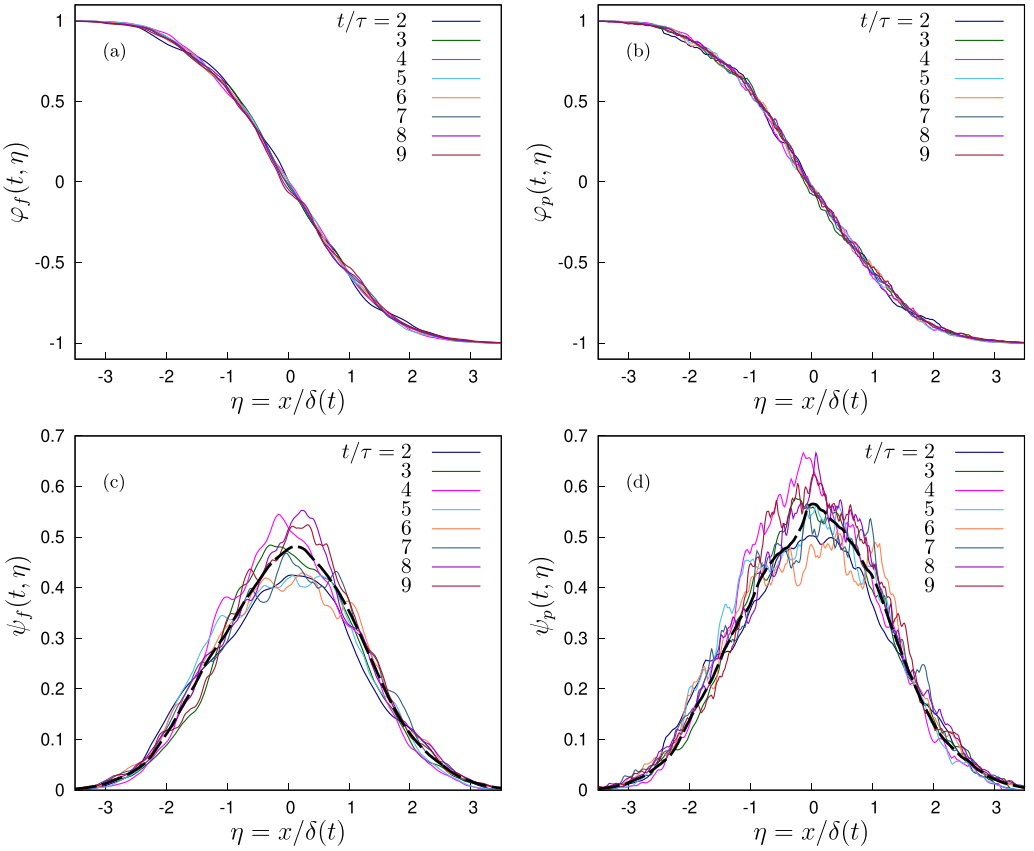


FIG. 7. Time evolution of the rescaled fluid (a) and particle (b) mean temperature and fluid (c) and particle (d) heat flux at $St = 1$ (the thick dashed line indicates the temporal average).

The temperature moment integral $\mathcal{I}_p$, while less sensitive, also reflects this behavior through the broader spatial distribution of enthalpy associated with the particles.

A key feature of inertial particles is their delayed thermal response, governed by the thermal relaxation time τ_ϑ. Unlike the fluid, which is governed by both advection and thermal diffusion, particles evolve thermally only through exchange with the fluid. This distinction leads to a lag in the particle temperature evolution, especially in regions with persistent temperature gradients. As a result, particles do not instantaneously follow the fluid temperature field, as reflected by the fact that $\mathcal{I}_p/\mathcal{I}_f$ exceeds one (Fig. 12), and may carry thermal energy across regions of strong gradients. This mechanism contributes to nonlocal heat transport, extending the range of enthalpy redistribution beyond that achievable by diffusion or fluid advection alone.

The governing equation for the system is the conservation of total enthalpy [Eq. (15)], which captures the combined contributions of the fluid and particle phases. Although the total enthalpy is governed by a single equation, the mean enthalpy of each phase evolves according to distinct dynamics: Eq. (14) for the fluid, incorporating advection and diffusion, and Eq. (13) for the particles, driven solely by thermal coupling to the surrounding fluid. Consequently, while the total enthalpy is conserved, its partition between phases is dynamic and influenced by the interplay of transport and relaxation timescales.

The effect of particle clustering on heat transfer is twofold. On the one hand, clustering near temperature gradients enhances velocity-temperature correlations and leads to stronger local enthalpy fluxes. On the other hand, closely grouped particles experience similar thermal environments,

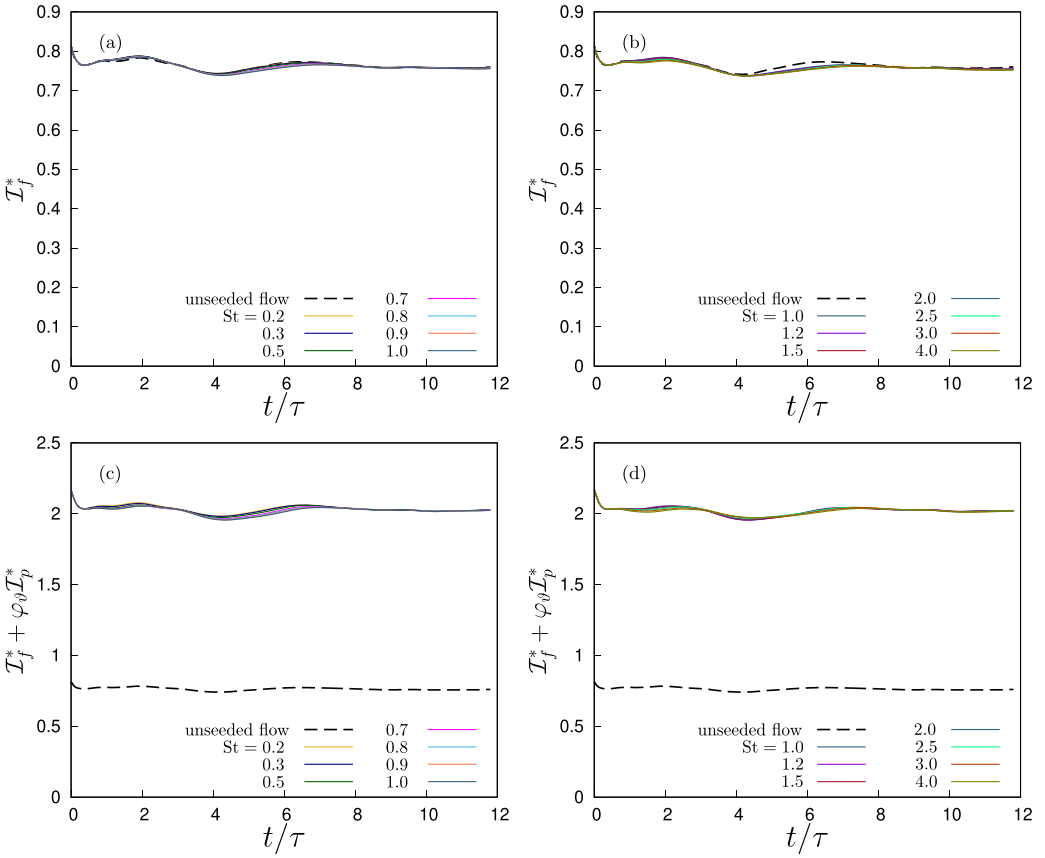


FIG. 8. First-order moment of mean total enthalpy integral, in two-way coupling regime relative to the first-order moment of fluid mean enthalpy integral in one-way coupling regime, particles with $St \leqslant 1$: (a) only fluid mean enthalpy integral (one- and two-way coupling) $\varphi_\vartheta = 0$; (b) total enthalpy integral, (fluid and particle mean enthalpy integrals) $\varphi_\vartheta = 1.664$.

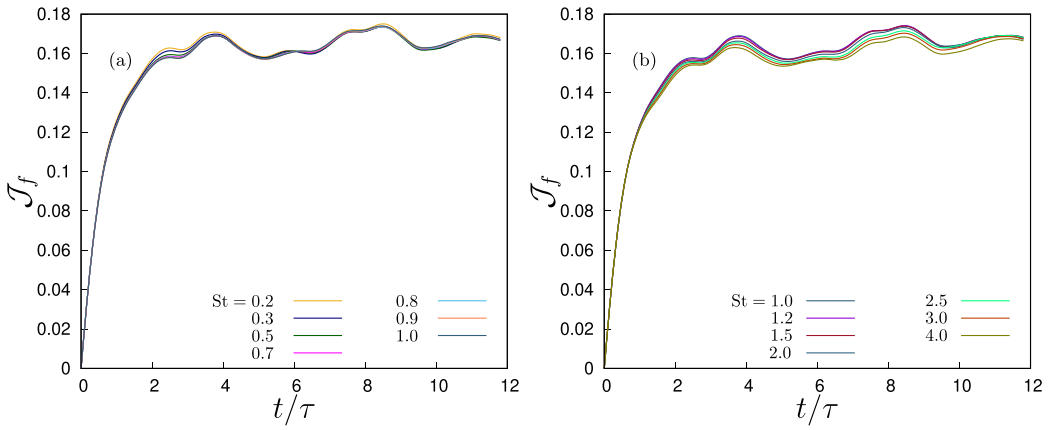


FIG. 9. Time variation of fluid flux integrals, $\mathcal{J}_f$ in two-way coupling regime: (a) particles with $St \leqslant 1$; (b) particles with $\mathrm{St} \geqslant 1$.

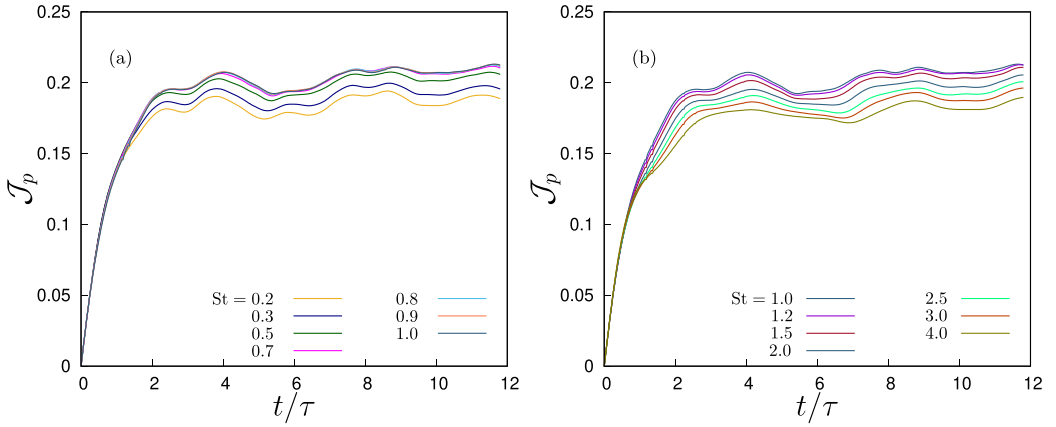


FIG. 10. Time variation of particle flux integrals, $\mathcal{J}_p$ in two-way coupling regime: (a) particles with $St \leqslant 1$; (b) particles with $\mathrm{St} \geqslant 1$.

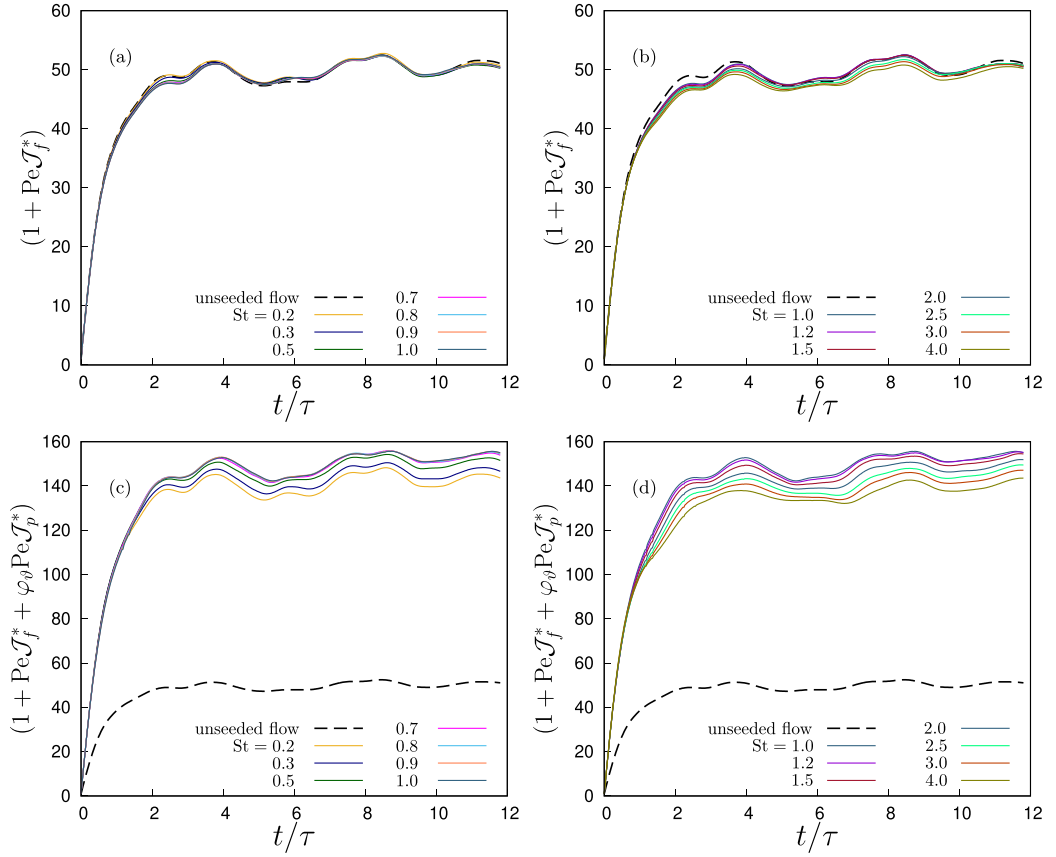


FIG. 11. Total heat flux integral, in two-way coupling regime relative to the fluid total heat flux integral unladen flow in one-way coupling, particles with $St \leqslant 1$: (a,b) total heat flux integrals for unladen flow in unseeded flow and particulate two-way thermally coupled with $\varphi_\vartheta = 0$; (c,d) total heat flux integrals in two-way coupling relative to unladen flow in one-way coupling, $\varphi_\vartheta = 1.664$.

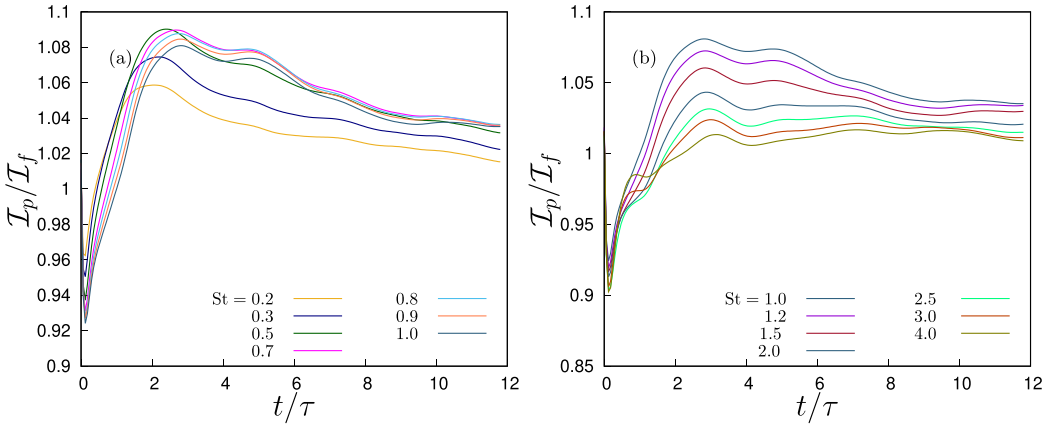


FIG. 12. Particle-to-fluid ratio of first-moment of mean temperature integrals $\mathcal{I}_p/\mathcal{I}_f$ in two-way coupling regime: (a) particles with $St \leqslant 1$; (b) particles with $\mathrm{St} \geqslant 1$.

limiting the effective temperature difference that drives heat exchange. As shown by Pouransari and Mani [38], this results in a reduction in heat transfer efficiency under intense clustering conditions, particularly around $\mathrm{St} \sim 1$, when particles respond to eddies near the Kolmogorov scale.

Despite this local limitation, the integral heat flux carried by the particles can exceed that of the fluid, as indicated by $\mathcal{J}_p/\mathcal{J}_f > 1$ (see Fig. 13), and by the corresponding increase in the Nusselt number (Fig. 14). This seemingly paradoxical outcome is resolved by considering the inertial delay of the particles: because their trajectories deviate from fluid streamlines, they are capable of transporting enthalpy across eddy structures, effectively enhancing heat transport over larger distances. As a result, substantial thermal inertia leads to improved thermal mixing, even when the mean local gradients are small.

Our DNS analysis confirms that all three components of the Nusselt number—diffusive, fluid convective, and particle—peak near $\mathrm{St} \sim 1$, albeit with different magnitudes. Compared to the unladen case, the diffusive contribution increases modestly ($\sim$3%), the fluid convective component increases by approximately 6%, and the particle term increases by more than 12%. While the overall

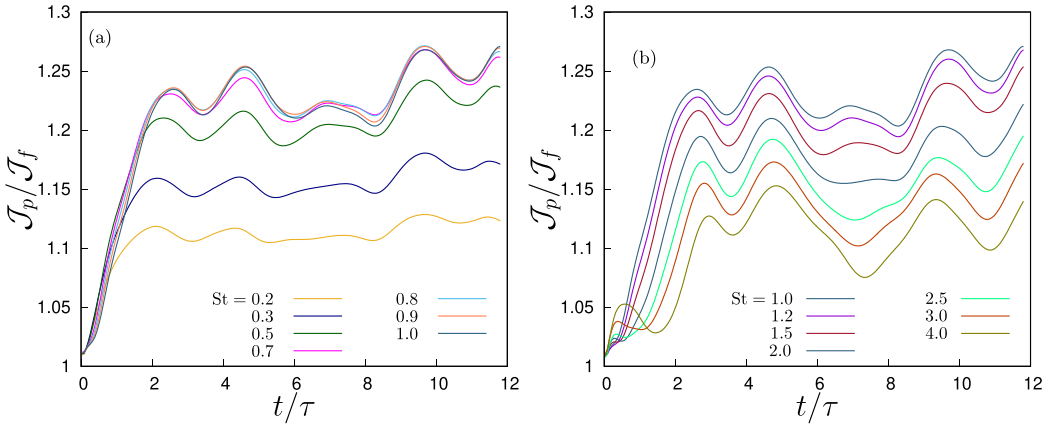


FIG. 13. Particle-to-fluid ratio of flux integrals $\mathcal{J}_p/\mathcal{J}_f$ in two-way coupling regime: (a) particles with $St \leqslant 1$; (b) particles with $\mathrm{St} \geqslant 1$.

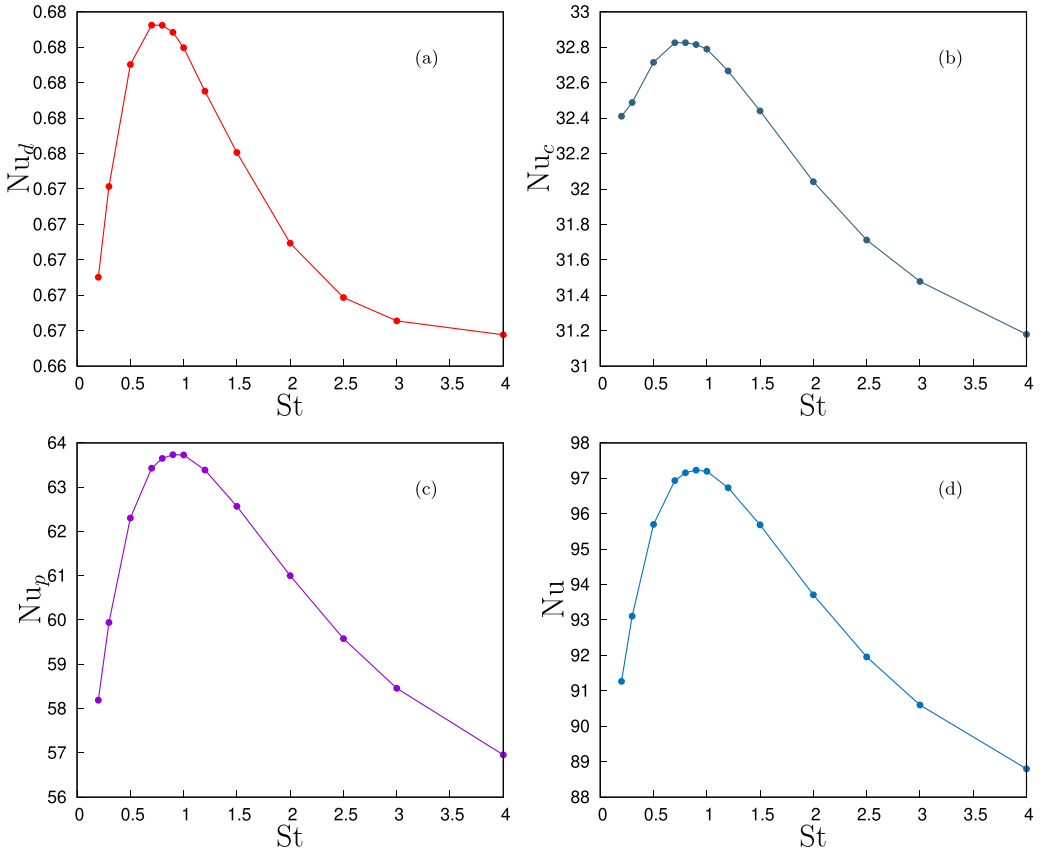


FIG. 14. Nusselt numbers in terms of Stokes number: (a) diffusive Nusselt number; (b) turbulent convective Nusselt number; (c) particle Nusselt number; (d) total Nusselt number.

change in the Nusselt number is modest (∼10%), this arises from a complex redistribution of heat fluxes and a modification of temperature structures, particularly the amplification of thermal moments in regions far from the core gradient. The trend that an increased particle thermal inertia increases the overall Nusselt number is in agreement with similar results in channel flow as observed by Liu *et al.* [42] for wall thermal Stokes number up to 266, even if the increase of the particle Nusselt number is associated to a reduction in the convective heat flux due to the damping of fluid fluctuations close to the wall where particle concentration is higher, particularly in the ejection regions, creating a sort of particle streaks. The suppression of near-wall ejection and sweeping motions, resulting also in reduced convective heat transfer, in a two-way momentum-coupled regime has been documented in many works, for any particle thermal capacity, including thermal tracers [42,44].

Importantly, although $\varphi_\vartheta > 0$ enables enhanced heat transfer under low volume fraction conditions, very high mass loadings can have the opposite effect. A nonmonotonic dependence on the thermal loading, analogous to the nonmonotonicity observed with mass loading [45], can be expected. As shown by Nakhaei and Lessani [46], particles can dampen turbulence and increase dissipation, thereby reducing the efficiency of convective transport. This suggests the existence of an optimal thermal loading that maximizes the net enthalpy transport while avoiding suppression of turbulent fluctuations.

These results offer a framework for optimizing nonisothermal particle-laden flows in engineering systems. By tuning the Stokes number and thermal inertia of particles, it becomes possible to control the balance of fluid and particle contributions to heat transfer. Although self-similarity is not an assumption in our general theoretical approach, based on the integral moments of the total enthalpy, which can also be used in non-self-similar flows, it can be verified *a posteriori* from the observed convergence of normalized flux and moment integrals.

Anyway, the self-similarity observed can be used to check the dynamics in phase space. Indeed, from Eq. (12), the particle flux integral can be expressed as

$$\mathcal{J}_p = \frac{\mathrm{d}}{\mathrm{d}t} \int \mathrm{d}x\, \mathrm{d}v\, \mathrm{d}\vartheta\, x\vartheta\, f_*(t, x, v, \vartheta).$$

The last integral is analogous to that of a single particle undergoing Brownian motion, which can be recovered by setting $\vartheta \equiv 1$, and measures the displacement of temperature (enthalphy) due to the stochastic forcing provided by fluid velocity and temperature fluctuations. A constant $\mathcal{J}_p$ implies a diffusive-like transport, and the integrated moments in the MTEI framework quantify the macroscopic diffusion of enthalpy.

V. CONCLUSIONS

We have investigated the thermal interaction between particles and fluid in a time-developing thermal mixing layer formed between two initially homothermal, homogeneous, and isotropic turbulent flows. This configuration serves as a simplified model for more complex thermally inhomogeneous turbulent systems. A phase-space analysis revealed the statistical structure of particle transport, highlighting the distinct behaviors of heat-releasing and heat-absorbing particles and the symmetries in their motion across the layer.

The core of our theoretical framework is based on the moment of total enthalpy integral (MTEI), which extends the approach used by [22] for boundary layer heat transfer. We formulated the first moment of the excess mean enthalpy relative to a static, purely diffusive state, capturing the combined influence of turbulent convection and particle-induced transport. This formulation yields integral expressions for both the fluid and particle contributions to heat transfer, providing a clear quantification of their individual and joint roles.

We used the self-similar solution of the fluid mean temperature field in the one-way thermal coupling regime as a reference state, analogous to laminar profiles in boundary layer analysis. This enabled us to assess how particles modify the evolution of the temperature field through their inertia and thermal response. The integral approach is robust against local measurement uncertainties and offers an independent estimate of global heat fluxes. It also serves as a tool to assess self-similarity and quantify deviations introduced by particle thermal inertia.

Analysis of DNS data [17] demonstrated that particle heat flux is influenced by both the mean temperature gradient and the transient dynamics of the mixing layer. The total heat transfer results from a combination of molecular diffusion, turbulent convection, and particle-mediated transport, each with distinct timescales and spatial patterns. While the flow tends toward a self-similar regime, particles introduce systematic corrections due to their thermal lag and clustering behavior.

Overall, this study establishes a consistent methodology for evaluating heat transfer in particle-laden turbulent flows, combining theoretical analysis and numerical data through the lens of the total enthalpy moment framework. Our findings show that particles can enhance thermal transport not only by directly carrying heat but also by altering fluid temperature distributions and enhancing turbulent correlations. This enhancement, however, is sensitive to both particle inertia and thermal properties, particularly the thermal mass fraction φ_ϑ. These insights provide a foundation for optimizing thermal management in multiphase systems, where balancing fluid and particle contributions is essential for controlling heat transfer efficiency.

ACKNOWLEDGMENTS

We wish to acknowledge HPC RIVR consortium [47] and EuroHPC JU [48] for awarding us access to the HPC system VEGA at IZUM [49], Maribor, Slovenia, under the PRACE EuroHPC Development Access (Project No. EHPC-DEV-2024D04-023). HPC@POLITO [50] is also gratefully acknowledged.

DATA AVAILABILITY

The data that support the findings of this article are not publicly available upon publication because it is not technically feasible, and/or the cost of preparing, depositing, and hosting the data would be prohibitive within the terms of this research project. The data are available from the authors upon reasonable request.

APPENDIX

We choose $L_0 = L_1/(2\pi)$ as a reference length, a reference velocity $U_0 = (4\varepsilon L_0)^{1/3}$ deduced from the imposed mean kinetic energy dissipation rate ε through the body force $\boldsymbol{f}$ (see [2]), and the temperature difference $T_1 - T_2$ as the reference temperature, so that we define the dimensionless velocity, pressure, and temperature as

$$\tilde{u}_i = \frac{u_i}{U_0}, \quad \tilde{p} = \frac{p - p_0}{\rho_f U_0^2}, \quad \tilde{T}_* = \frac{T_*}{T_1 - T_2},$$

where p_0 is a reference mean pressure; T_* is the fluctuating part of the temperature, defined by (2). The dimensionless form of the governing equations (3)–(5) for the carrier flow is therefore

$$\frac{\partial \tilde{u}_i}{\partial \tilde{x}_i} = 0, \tag{A1}$$

$$\frac{\partial \tilde{u}_i}{\partial \tilde{t}} + \tilde{u}_j \frac{\partial \tilde{u}_i}{\partial \tilde{x}_j} = -\frac{\partial \tilde{p}}{\partial \tilde{x}_i} + \frac{1}{\mathrm{Re}} \frac{\partial^2 \tilde{u}_i}{\partial \tilde{x}_j \partial \tilde{x}_j} + \tilde{f}_{u,i}, \tag{A2}$$

$$\frac{\partial \tilde{T}_*}{\partial \tilde{t}} + \tilde{u}_j \frac{\partial \tilde{T}_*}{\partial \tilde{x}_j} = -\frac{1}{4\pi} \tilde{u}_3 + \frac{1}{\mathrm{RePr}} \frac{\partial^2 \tilde{T}_*}{\partial \tilde{x}_j \partial \tilde{x}_j} + \tilde{C}_T, \tag{A3}$$

where $\mathrm{Re} = (4\varepsilon L_0^4)^{1/3}/\nu$ is the Reynolds number, and $\mathrm{Pr} = \kappa/\nu$ is the Prandtl number. By choosing $L_2 = L_3 = 2L_1$, these equations are solved in a $(0, 2\pi) \times (0, 2\pi) \times (-2\pi, 2\pi)$ domain with periodic boundary conditions on $\tilde{u}_i$, $\tilde{p}$, $\tilde{T}_*$. Analogously, the dimensionless position, velocity, and temperature of particles are defined as

$$\tilde{X}_{p,i} = \frac{X_{p,i}}{L_0}, \quad \tilde{V}_{p,i} = \frac{V_{p,i}}{U_0}, \quad \tilde{\Theta}_{p,i} = \frac{\Theta_{p,i}}{T_1 - T_2},$$

so that the particle governing equations (1) become, in dimensionless form,

$$\frac{\mathrm{d}}{\mathrm{d}\tilde{t}} \begin{Bmatrix} \tilde{X}_{p,i}(\tilde{t}) \\ \tilde{V}_{p,i}(\tilde{t}) \\ \tilde{\Theta}^*_p(\tilde{t}) \end{Bmatrix} = \begin{bmatrix} 0 & 1 & 0 \\ 0 & -1/\tilde{\tau}_v & 0 \\ 0 & -\frac{1}{4\pi}\delta_{i3} & -1/\tilde{\tau}_\vartheta \end{bmatrix} \begin{Bmatrix} \tilde{X}_{p,i}(\tilde{t}) \\ \tilde{V}_{p,i}(\tilde{t}) \\ \tilde{\Theta}^*_p(\tilde{t}) \end{Bmatrix} + \begin{bmatrix} 0 \\ (1/\tilde{\tau}_v)\tilde{\boldsymbol{u}}(\tilde{t}, \tilde{\boldsymbol{X}}_p) \\ (1/\tilde{\tau}_\vartheta)\tilde{T}_*(\tilde{t}, \tilde{\boldsymbol{X}}_p) \end{bmatrix}, \tag{A4}$$

where the dimensionless particle relaxation times [Eq. (2)] are given by

$$\tilde{\tau}_v = \mathrm{St}\frac{\tau_\eta U_0}{L_0} = 2\,\mathrm{St}\,\mathrm{Re}^{-1/2}, \quad \tilde{\tau}_\vartheta = \mathrm{St}_\vartheta \frac{\tau_\eta U_0}{L_0} = 2\,\mathrm{St}_\vartheta\,\mathrm{Re}^{-1/2}. \tag{A5}$$

Finally, the dimensionless particle feedback term $\tilde{C}_T$ can be expressed as

$$\tilde{C}_T = \varphi_\vartheta \frac{16\pi^3}{N_p} \sum_{p=1}^{N_p} \frac{\tilde{T}_*(\tilde{t}, \tilde{\boldsymbol{x}}) - \tilde{\Theta}_p^*(\tilde{t})}{\tilde{\tau}_\vartheta} \tilde{\delta}(\tilde{\boldsymbol{x}} - \tilde{\boldsymbol{X}}_p),$$

where φ_ϑ is the particle-to-fluid heat capacity ratio. A deterministic body force $\tilde{\boldsymbol{f}}$, a linear function of the velocity, is used in Eq. (A2) to keep the velocity field statistically steady by injecting energy at a single wave number $\tilde{k}_f$ (see also [2,17] for further details about the forcing). In dimensionless form, its representation in the Fourier space is given by

$$\hat{\tilde{\boldsymbol{f}}}(\tilde{t}, \tilde{\boldsymbol{\kappa}}) = \frac{1}{4} \frac{\hat{\tilde{\boldsymbol{u}}}(\tilde{t}, \tilde{\boldsymbol{\kappa}})}{\sum_{|\tilde{\boldsymbol{\kappa}}|=\tilde{\kappa}_f} |\hat{\tilde{\boldsymbol{u}}}(\tilde{t}, \tilde{\boldsymbol{\kappa}})|^2} \tilde{\delta}(|\tilde{\boldsymbol{\kappa}}| - \tilde{\kappa}_f).$$

This dimensionless formulation is the one actually solved by the numerical code.

[1] I. Saito, T. Watanabe, and T. Gotoh, Modulation of fluid temperature fluctuations by particles in turbulence, J. Fluid Mech. **931**, A6 (2022).

[2] M. Carbone, A. D. Bragg, and M. Iovieno, Multiscale fluid-particle thermal interaction in isotropic turbulence, J. Fluid Mech. **881**, 679 (2019).

[3] M. Carbone and M. Iovieno, Accurate direct numerical simulation of two-way coupled particle-laden flows through the nonuniform Fast Fourier Transform, IJSSE **10**, 191 (2020).

[4] L. I. Zaichik and V. M. Alipchenkov, Pair dispersion and preferential concentration of particles in isotropic turbulence, Phys. Fluids **15**, 1776 (2003).

[5] L. I. Zaichik and V. M. Alipchenkov, Statistical models for predicting pair dispersion and particle clustering in isotropic turbulence and their applications, New J. Phys. **11**, 103018 (2009).

[6] J. Chun, D. L. Koch, S. L. Rani, A. Ahluwalia, and L. R. Collins, Clustering of aerosol particles in isotropic turbulence, J. Fluid Mech. **536**, 219 (2005).

[7] J. Bec, H. Homann, and G. Krstulovic, Clustering, fronts, and heat transfer in turbulent suspensions of heavy particles, Phys. Rev. Lett. **112**, 234503 (2014).

[8] J. Bec and R. Vallée, Homogeneous turbophoresis of heavy inertial particles in turbulent flow, J. Fluid Mech. **999**, A83 (2024).

[9] L. Chen, S. Goto, and J. C. Vassilicos, Turbulent clustering of stagnation points and inertial particles, J. Fluid Mech. **553**, 143 (2006).

[10] S. W. Coleman and J. C. Vassilicos, A unified sweep-stick mechanism to explain particle clustering in two- and three-dimensional homogeneous, isotropic turbulence, Phys. Fluids **21**, 113301 (2009).

[11] E. Meneguz and M. W. Reeks, Statistical properties of particle segregation in homogeneous isotropic turbulence, J. Fluid Mech. **686**, 338 (2011).

[12] S. Lee and C. Lee, Identification of a particle collision as a finite-time blowup in turbulence, Sci. Rep. **13**181 (2023).

[13] H. R. Zandi Pour and M. Iovieno, On the formation of thermal caustics in turbulent particle-laden flows, Phys. Fluids **36**, 121711 (2024).

[14] Z. Warhaft, Passive scalars in turbulent flows, Annu. Rev. Fluid Mech. **32**, 203 (2000).

[15] L. Mydlarski and Z. Warhaft, Passive scalar statistics in high Péclet number grid turbulence, J. Fluid Mech. **358**, 135 (1998).

[16] M. Iovieno, S. Di Savino, L. Gallana, and D. Tordella, Mixing of a passive scalar across a thin shearless layer: Concentration of intermittency on the sides of the turbulent interface, J. Turbul. **15**, 311 (2014).

[17] H. R. Zandi Pour and M. Iovieno, Heat transfer in a non-isothermal collisionless turbulent particle-laden flow, Fluids **7**, 345 (2022).

[18] H. R. Zandi Pour and M. Iovieno, Heat transfer enhancement by suspended particles in a turbulent shearless flow, in *33rd Congress of the International Council of the Aeronautical Sciences (ICAS 2022), Stockholm, Sweden* (ICAS, 2022), Vol. 4, pp. 2452–2463.
[19] H. R. Zandi Pour and M. Iovieno, The role of particle inertia and thermal inertia in heat transfer in a non-isothermal particle-laden turbulent flow, Fluids **9**, 29 (2024).
[20] A. Halle, S. Colombi, and S. Peirani, Phase-space structure analysis of self-gravitating collisionless spherical systems, Astronomy & Astrophysics **621**, A8 (2019).
[21] A. Elnahhas and P. L. Johnson, On the enhancement of boundary layer skin friction by turbulence: An angular momentum approach, J. Fluid Mech. **940**, A36 (2022).
[22] A. Kianfar, A. Elnahhas, and P. L. Johnson, Quantifying how turbulence enhances boundary layer skin friction and surface heat transfer, AIAA J. **61**, 3900 (2023).
[23] A. Kianfar and P. L. Johnson, Moment of momentum integral analysis of turbulent boundary layers with pressure gradient, J. Fluid Mech. **1002**, A29 (2025).
[24] A. Kianfar, M. Di Renzo, C. Williams, A. Elnahhas, and P. L. Johnson, Angular momentum and moment of total enthalpy integral equations for high-speed boundary layers, Phys. Rev. Fluids **8**, 054603 (2023).
[25] A. A. Townsend, *The Structure of Turbulent Shear Flow* (Cambridge University Press, Cambridge, UK, 1980).
[26] T. Wei, Self-similarity analysis of turbulent wake flows, J. Fluids Eng. **139**, 051203 (2017).
[27] X.-L. Xiong, S. Laima, H. Li, and Y. Zhou, Self-similarity in single-point turbulent statistics across different quadrants in turbulent rotor wakes, Phys. Rev. Fluids **9**, 054608 (2024).
[28] M. R. Maxey and J. J. Riley, Equation of motion for a small rigid sphere in a nonuniform flow, Phys. Fluids **26**, 883 (1983).
[29] R. Gatignol, Faxen formulae for a rigid particle in an unsteady non-uniform Stokes flow, J. Mec. Theor. Appl. **2**, 143 (1983).
[30] H. Homann and J. Béc, Finite-size effects in the dynamics of neutrally buoyant particles in turbulent flow, J. Fluid Mech. **651**, 81 (2010).
[31] V. Armenio and V. Fiorotto, The importance of the forces acting on particles in turbulent flows, Phys. Fluids **13**, 2437 (2001).
[32] J.-P. Minier and C. Henry, The dynamics of discrete particles in turbulent flows: Open issues and current challenges in statistical modeling, arXiv:2311.01921 [physics.flu-dyn].
[33] J. A. K. Horwitz, S. Ganguli, and S. K. Lele, Settling of two-way momentum and energy coupled particles subject to Boussinesq and non-Boussinesq heating, Theor. Comput. Fluid Dyn. **35**, 539 (2021).
[34] S. Sundaram and L. R. Collins, Numerical considerations in simulating a turbulent suspension of finite-volume particles, J. Comput. Phys. **124**, 337 (1996).
[35] H. R. Zandi Pour and M. Iovieno, The impact of collisions on heat transfer in a particle-laden shearless turbulent flow, Journal of Fluid Flow, Heat and Mass Transfer **10**, 140 (2023).
[36] H. R. Zandi Pour and M. Iovieno, On the heat transfer in particle-laden turbulent flows: The effect of collision in an anisothermal regime, in *Proceedings of the 9th World Congress on Mechanical, Chemical, and Material Engineering, MCM 2023* (Brunel University, London, UK, 2023), p. HTFF 126-1.
[37] C. S. Ng, V. Spandan, R. Verzicco, and D. Lohse, Non-monotonic transport mechanisms in vertical natural convection with dispersed light droplets, J. Fluid Mech. **900**, A34 (2020).
[38] H. Pouransari and A. Mani, Particle-to-fluid heat transfer in particle-laden turbulence, Phys. Rev. Fluids **3**, 074304 (2018).
[39] I. Saito, T. Watanabe, and T. Gotoh, A new time scale for turbulence modulation by particles, J. Fluid Mech. **880**, R6 (2019).
[40] M. Carbone and M. Iovieno, Application of the non-uniform Fast Fourier Transform to the Direct Numerical Simulation of two-way coupled turbulent flows, WIT Trans. Eng. Sci. **120**, 237 (2018).
[41] J.-P. Minier, M. Ferrand, and C. Henry, Statistical modeling of particle transport in turbulent flows, in *Understanding Turbulent Systems: Progress in Particle Dynamics Modeling* (Springer Nature Switzerland, Cham, 2025) pp. 75–95.
[42] C. Liu, S. Tang, and Y. Dong, Effect of inertial particles with different specific heat capacities on heat transfer in particle-laden turbulent flow, Appl. Math. Mech. **38**, 1149 (2017).

[43] M. Pan, L. Shen, Q. Zhou, and Y. Dong, Particle transport and turbulence modification in unstably stratified mixed convection within a horizontal channel, Int. J. Heat Mass Transf. **236**, 126377 (2025).
[44] Y. Pei, W. Chen, X.-L. Xiong, X. Xu, and Y. Zhou, Direct numerical simulation of turbulent flow and heat transfer in a particle-laden turbulent channel flow, Int. J. Heat Fluid Flow **110**, 109617 (2024).
[45] T. Zhou, L. Zhao, W. Huang, and C. Xu, Non-monotonic effect of mass loading on turbulence modulations in particle-laden channel flow, Phys. Fluids **32**, 043304 (2020).
[46] M. Nakhaei and B. Lessani, Effects of solid inertial particles on the velocity and temperature statistics of wall bounded turbulent flow, Int. J. Heat Mass Transf. **106**, 1014 (2017).
[47] www.hpc-rivr.si
[48] eurohpc-ju.europa.eu
[49] www.izum.si
[50] www.hpc.polito.it